

# Incident Direction Independent Wave Propagation and Unidirectional Lasing

L. Jin<sup>1,\*</sup> and Z. Song<sup>1</sup>

<sup>1</sup>*School of Physics, Nankai University, Tianjin 300071, China*

We propose an incident direction independent wave propagation generated by properly assembling different unidirectional destructive interferences (UDIs), which is a consequence of the appropriate match between synthetic magnetic fluxes and the incident wave vector. Single-direction lasing at spectral singularity is feasible without introducing nonlinearity. UDI allows unidirectional lasing and unidirectional perfect absorption; when they are combined in a parity-time symmetric manner, the spectral singularities vanish with bounded reflections and transmissions. Furthermore, the simultaneous unidirectional lasing and perfect absorption for incidences from opposite directions is created. Our findings provide insights into light control and may shed light on the explorations of desirable functionality in fundamental research and practical applications.

*Introduction.*—Parity-time ( $\mathcal{PT}$ ) symmetry has been theoretically and experimentally investigated in a variety of non-Hermitian systems [1–22], non-Hermiticity controls the exact and broken  $\mathcal{PT}$ -symmetric phases [18–22]. The phase transition points are exceptional points [23–27] utilized for sensing enhancement [13, 28, 30–32]. The topologies of exceptional points are distinct [33–37]. Spectral singularities (SS) in scattering systems belong to another type of non-Hermitian singularities, at which eigenstate completeness is spoiled [38, 39]; incident waves from opposite directions at an appropriate phase match are perfectly absorbed in a coherent perfect absorber [3, 40, 41, 43–48].

Non-Hermitian character causes unidirectionality [4, 5, 49, 52–54], the fundamental mechanism of which differs from that created by chiral light-matter interaction [55–59]. Typical phenomena include unidirectional reflectionlessness [4, 49] and unidirectional spectral singularity that allows unidirectional perfect absorption (UPA) and unidirectional lasing (UL) [5, 52]; however, the transmissions there protected by symmetry are reciprocal [1, 2, 9, 61]. Nonreciprocal transmission is indispensable for optical information processing. Nonreciprocity, implemented via magneto-optic effect [64] and optical nonlinearity [65], has been created based on various strategies in linear and magnetic-free devices [66, 67], in single-photon level [68, 69], and even in acoustics [70]. Benefitted from synthetic magnetic flux realized for photons [71–79] and progress in non-Hermitian physics [22], non-Hermiticity associated with synthetic magnetic flux induces nonreciprocal transmission in linear photonic lattices [80–82].

In this Letter, we propose an incident direction independent wave propagation, which is an extraordinary asymmetry in both *reflectivity* and *transmittivity* that stemmed from the unidirectional destructive interference (UDI); single-direction lasing occurs at the SS, where an incidence from either side induces a UL toward the same direction. The appropriate match between synthetic magnetic fluxes in different functional UDIs creates many intriguing unidirectional phenomena beyond one-way propagation, UPA, and UL [82]. With judiciously

chosen synthetic magnetic fluxes, detunings, and the gain or loss of side-coupled resonators, the SS exhibits UPA or UL; their coincidence leads to an SS elimination under  $\mathcal{PT}$  symmetry. Furthermore, a simultaneous unidirectional lasing and perfect absorption for incidences from opposite sides is feasible by assembling different unidirectional elements. These novel wave propagation phenomena facilitate various applications of non-Hermitian metamaterials without introducing nonlinearity [83–86].

*Model.*—We consider a one-dimensional uniformly coupled passive resonator chain in Fig. 1(a) with identical resonant frequency  $\omega_c$ ; the primary resonators (round-shaped) are evanescently coupled through the auxiliary resonators (stadium-shaped), which are antiresonant with the primary resonators. The coupling strength  $J = 1$  is set to be unity. A resonator is side-coupled to the resonator chain with one asymmetric coupling, which is introduced through the optical path length difference  $2\Delta x$  in the tunneling between resonators  $\alpha$  and 0 [76]. An extra direction-dependent phase factor  $e^{\pm i\phi_\alpha}$  is equivalently induced in the effective coupling between resonators  $\alpha$  and 0, resulting in a synthetic magnetic flux  $\phi_\alpha = 2\pi\Delta x/\lambda \equiv (-e/\hbar) \oint \vec{A}_\alpha \cdot d\vec{l}$  in the triangle that associated with a vector potential  $\vec{A}_\alpha$  [73, 74, 79], where  $\lambda$  is the resonant wavelength [77]. The resonators support the counterclockwise (CCW) and clockwise (CW) modes, they experience opposite synthetic magnetic fluxes. The CCW mode is analyzed without loss of generality, the CW mode is discussed as well.

The frequency detuning (net gain or loss) of resonator  $\alpha$  is represented by the real (imaginary) part of  $V_\alpha$ . The loss is the dissipation  $\omega_c/(2Q_\alpha)$  caused by the interaction between resonator  $\alpha$  and its environment, where  $Q_\alpha$  is the quality factor. The gain is induced by pumping the ions doped in the resonator [14, 20]. Assuming a weak pump that far away from gain saturation with white noise [87, 88], both processes are Markovian and characterized by Lindblad master equation [89, 90], where the gain and loss are modeled by constants [5, 14, 20, 91, 92].

We consider an ideal case of resonators with negligible backscattering [93]. In the coupled-mode theory [6, 7],

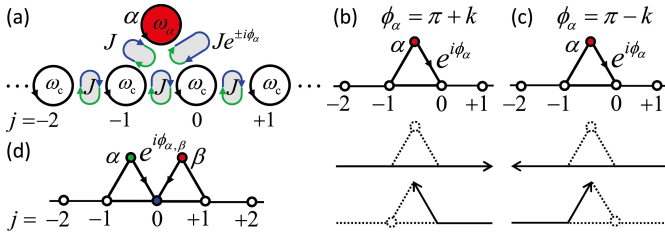


FIG. 1. (a) Schematic of uniform resonator chain with one side-coupled resonator,  $\omega_\alpha = \omega_c + V_\alpha$ . The blue and green arrows indicate the optical path lengths for counterclockwise mode (black arrow) photons tunneling between resonators in opposite directions. (b) Right-UPA: right perfect absorption and left resonant transmission. (c) Left-UPA: left perfect absorption and right resonant transmission. The upper panels illustrate UPA configurations with opposite synthetic magnetic fluxes,  $k$  is the incident wave vector and  $V_\alpha = -e^{ik}$ ; the central panels illustrate destructive interference at the side-coupled resonator  $\alpha$  from one incident direction; and the lower panels illustrate perfect absorption from the opposite incident direction, the dotted line indicates the equivalently decoupled part. (d) Schematic of uniform resonator chain with two side-coupled resonators.  $j$  is the resonator index,  $\omega_{\alpha,0,\beta} = \omega_c + V_{\alpha,0,\beta}$ .

the equation of motion for resonators  $j \neq -1, 0$ , and  $\alpha$  in the system illustrated in Fig. 1(a) is

$$i \frac{d\psi_j}{dt} = \omega_c \psi_j - \psi_{j-1} - \psi_{j+1}, \quad (1)$$

otherwise,

$$i \frac{d\psi_{-1}}{dt} = \omega_c \psi_{-1} - \psi_{-2} - \psi_0 - \psi_\alpha, \quad (2)$$

$$i \frac{d\psi_\alpha}{dt} = (\omega_c + V_\alpha) \psi_\alpha - \psi_{-1} - e^{-i\phi_\alpha} \psi_0, \quad (3)$$

$$i \frac{d\psi_0}{dt} = \omega_c \psi_0 - \psi_{-1} - \psi_1 - e^{i\phi_\alpha} \psi_\alpha, \quad (4)$$

where  $\psi_j = f_j e^{-i\omega t}$  is the field amplitude and  $f_j$  is the steady-state wave function of resonator  $j$  in the elastic scattering process with  $f_j = Ae^{ikj} + Be^{-ikj}$  ( $j < 0$ ) and  $f_j = Ce^{ikj} + De^{-ikj}$  ( $j > 0$ ).  $k \in [-\pi, \pi]$  is the dimensionless Bloch wave vector [1, 2, 5, 80]. The resonator chain supported dispersion relation is  $\omega = \omega_c - 2J \cos k$  [5, 76], a resonant incidence with frequency  $\omega_c$  has the wave vector  $k = \pi/2$ .

*Unidirectional destructive interference.*—Synthetic magnetic flux affects the interference, breaks the system symmetry and the reciprocity of transmission [93]. When synthetic magnetic flux matches the incident wave vector  $\phi_\alpha = \pi \pm k$ , incidences from both sides are reflectionless. The side-coupled resonator  $\alpha$  is equivalently isolated for the left (right) incidence because of the destructive interference induced by  $\phi_\alpha = \pi + k$  ( $\phi_\alpha = \pi - k$ ); the wave function at resonator  $\alpha$  is zero. For the right (left) incidence, the wave function of resonator  $\alpha$  does not

vanish, it varies according to  $V_\alpha$  and affects the right (left) transmission.

The reflection and transmission coefficients are  $r_L = B/A$ ,  $t_L = C/A$  for the left incidence ( $D = 0$ ); and  $r_R = C/D$ ,  $t_R = B/D$  for the right incidence ( $A = 0$ ). The scattering matrix characterizes the relationship between input and output [9, 48]

$$\begin{pmatrix} B \\ C \end{pmatrix} = S \begin{pmatrix} A \\ D \end{pmatrix}. \quad (5)$$

Here, the scattering matrix is asymmetric [93]

$$S = \begin{pmatrix} r_L & t_R \\ t_L & r_R \end{pmatrix} = \begin{pmatrix} 0 & (e^{ik} + V_\alpha) / (e^{-ik} + V_\alpha) \\ 1 & 0 \end{pmatrix}, \quad (6)$$

induced by the asymmetric coupling. In Hermitian systems (real  $V_\alpha$ ), the transmittivity is  $|t_L|^2 = |t_R|^2 = 1$ ;  $f_\alpha$  vanishes for the left incidence, but is nonzero for the right incidence. In non-Hermitian systems (complex  $V_\alpha$ ), the transmittivity is asymmetric,  $|t_L|^2 \neq |t_R|^2$ .

At  $\phi_\alpha = \pi + k$ , the scattering of left incidence with wave vector  $k$  is fixed even though  $V_\alpha$  varies; the perfect absorption occurs for the right incidence when  $V_\alpha = -e^{ik}$  [Fig. 1(b)]; in contrast to an isolator [9], the scattering matrix  $S = \begin{pmatrix} 0 & 0 \\ 1 & 0 \end{pmatrix}$  is for the CCW mode and its transpose  $S^T$  is for the CW mode [93]. The wave function for the right incidence consists of an incoming wave that is completely absorbed at resonator  $\alpha$  without reflection, i.e.,  $f_j = 0$  ( $j < 0$ ),  $f_j = e^{-ikj}$  ( $j \geq 0$ ), and  $f_\alpha = -1$ ;  $r_L = r_R = t_R = 0$  and  $|t_L| = 1$ , behaving similarly in a coupled helical waveguide design [80] but differently in the transmissionless-UPA [52]. When the synthetic magnetic flux is opposite  $\phi_\alpha = \pi - k$ , the wave function is a left-right mirror reflection of that at  $\phi_\alpha = \pi + k$ , where resonator  $\alpha$  is isolated for the right incidence [Fig. 1(c)]. A right-UPA for the CCW mode is a left-UPA for the CW mode, UPA realizes chiral mode isolation [64–66].

UL occurs at  $V_\alpha = -e^{-ik}$  when  $t_R$  diverges [5, 38, 96], where resonator  $\alpha$  has an equal amount of gain in contrast to the UPA. The wave function for the right incidence consists of an outgoing wave that satisfies the boundary condition of lasing without any injection, i.e.,  $f_j = e^{-ikj}$  ( $j < 0$ ),  $f_j = 0$  ( $j \geq 0$ ), and  $f_\alpha = 1$ .

*Incident direction independent wave propagation.*—UDI facilitates the design of optical control devices, leading to an isolation of side-coupled resonator in one incident direction and providing an opportunity to unidirectionally manipulate the waves. When assembling one more side-coupled resonator, the cooperation between synthetic magnetic fluxes in UDIs enriches the intriguing asymmetric dynamics [82].

The equations of motion for the configuration of two

side-coupled resonators [Fig. 1(d)] are Eqs. (15-17) and

$$i \frac{d\psi_0}{dt} = (\omega_c + V_0) \psi_0 - \psi_{-1} - \psi_1 - e^{i\phi_\alpha} \psi_\alpha - e^{i\phi_\beta} \psi_\beta \quad (7)$$

$$i \frac{d\psi_\beta}{dt} = (\omega_c + V_\beta) \psi_\beta - \psi_1 - e^{-i\phi_\beta} \psi_0, \quad (8)$$

$$i \frac{d\psi_1}{dt} = \omega_c \psi_1 - \psi_0 - \psi_2 - \psi_\beta, \quad (9)$$

where the real (imaginary) parts of  $V_\beta$  and  $V_0$  represent the frequency detunings (net gains or losses) of resonators  $\beta$  and 0, respectively.

At fixed synthetic magnetic fluxes  $\phi_\alpha = \phi_\beta = \pi + k$ , Figs. 2(a) and 2(b) illustrate the wave propagation for opposite incidences. In Fig. 2(a), the wave resonantly transmits at resonator  $\alpha$  because of the destructive interference. Then, the transmitted wave is scattered at resonator 0, corresponding reflection and transmission coefficients are  $r_0 = V_0/(2i \sin k - V_0)$  and  $t_0 = r_0 + 1$  [97]. The reflected portion (cyan arrow) passes through resonator  $\alpha$  from the right side without reflection (green arrow) and forms the left reflection; the transmitted portion (purple arrow) passes through resonator  $\beta$  from the left side without reflection (red arrow) and forms the left transmission. The green (red) arrow represents the reflectionless transmission modulated by resonator  $\alpha$  ( $\beta$ ). The reflection and transmission coefficients are [93]:

$$r_L = r_0 \frac{e^{ik} + V_\alpha}{e^{-ik} + V_\alpha}, t_L = t_0 \frac{e^{ik} + V_\beta}{e^{-ik} + V_\beta}; \quad (10)$$

$$r_R = r_0 \frac{e^{ik} + V_\beta}{e^{-ik} + V_\beta}, t_R = t_0 \frac{e^{ik} + V_\alpha}{e^{-ik} + V_\alpha}. \quad (11)$$

The synthetic magnetic fluxes allow that the propagating waves in the left (right) chain after scattering are  $V_{\beta(\alpha)}$  independent, regardless of the incident direction. This enables an incident direction independent wave propagation when  $|r_0| = |t_0|$  (requiring  $|2 \sin k/V_0| = 1$ ): the left reflectivity and transmittivity equal to the right transmittivity and reflectivity, respectively.

$$|r_L|^2 = |t_R|^2, |t_L|^2 = |r_R|^2. \quad (12)$$

The left- and right-going propagating wave *intensities* after scattering are identical for incidences impinging from both directions and are separately tuned by  $V_\alpha$  and  $V_\beta$ , respectively. The wave impinging from either direction is equally divided at resonator 0 with  $|r_0| = |t_0| = \sqrt{1/(2 - 2 \sin \varphi)}$  when  $V_0 = 2e^{i\varphi} \sin k$ .

The incident direction independent wave propagation occurs at

$$\phi_\alpha = \phi_\beta = \pi + k, V_0 = 2e^{i\varphi} \sin k. \quad (13)$$

Resonator  $\beta$  ( $\alpha$ ) being  $V_{\beta(\alpha)} = -e^{ik}$  induces a perfect absorption of the right- (left-) going propagating wave, except that the system is at the SS when  $V_0 = 2i \sin k$ , where lasing is bidirectional; or when  $V_{\alpha(\beta)} = -e^{-ik}$ ,

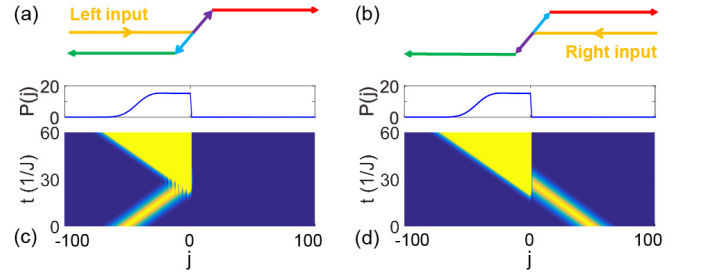


FIG. 2. (a, b) Schematic of the incident direction independent wave propagation. (c, d) Simulations of single-direction lasing at  $V_\alpha = -e^{-ik}$ ,  $V_\beta = -e^{ik}$  in Fig. 1(d). The Gaussian wave packet is  $|\Psi(0, j)\rangle = (\sqrt{\pi}/\sigma)^{-1/2} \sum_j e^{-(\sigma^2/2)(j-N_c)^2} e^{ik_c j} |j\rangle$ , centered at  $N_c$ , where  $k_c = \pi/3$  is the wave vector,  $\sigma = 0.1$ , and  $j$  is the resonator index. The resonator chain is cut at  $j = \pm 100$ . The blue curves in (c, d) depict the wave intensities  $P(j) = |\Psi(t, j)|^2$  at time  $t = 60/J$ . Other parameters are  $\phi_\alpha = \phi_\beta = \pi + k$ ,  $V_0 = -2i \sin k$ , and  $k = \pi/3$ .

where the lasing is unidirectional toward the left (right) and the propagating wave in the right (left) chain vanishes after scattering, e.g., UL occurs when  $V_\alpha = -e^{-ik}$ ,  $V_\beta = -e^{ik}$ , and  $V_0 = -2i \sin k$ ; the lasing wave is emitted from the left chain, independent of the incident direction; and the right-going propagating wave vanishes, being absorbed at resonator  $\beta$ . The reflection and transmission coefficients satisfy

$$|r_L| = |t_R| \rightarrow \infty, t_L = r_R = 0. \quad (14)$$

The wave function is  $f_j = e^{-ikj}$  ( $j < 0$ ),  $f_j = 0$  ( $j \geq 0$ ),  $f_\alpha = 1$ , and  $f_\beta = 0$ ; consisting of the outgoing wave in the left chain. For an incidence from either direction, the lasing wave is emitted in a single direction: leftward. The simulation of single-direction lasing is depicted in Figs. 2(c) and 2(d). A Gaussian wave packet excites the wave emission, characterized by a Gaussian error function and its intensity increases linearly [10]. At  $V_0 = 2i \sin k$ , lasing is bidirectional when  $V_{\alpha,\beta} \neq -e^{ik}$ ; the wave emission is symmetric if  $V_{\alpha,\beta}$  is real, but asymmetric if complex  $V_\alpha \neq V_\beta$ ; when  $V_{\alpha(\beta)} = -e^{ik}$ , the wave emission is absorbed at resonator  $\alpha$  ( $\beta$ ) and the lasing becomes unidirectional with vanishing emission toward the left (right). When  $V_\alpha = V_\beta = -e^{-ik}$ , lasing is bidirectional and  $V_0$  controls the asymmetry of lasing amplitude.

Another intriguing application is the one-way propagation at  $V_\alpha = -\cos k + 3^{\pm 1} i \sin k$ ,  $V_\beta = -e^{ik}$ , and  $V_0 = -2i \sin k$  previously designed using different strategies [82–84], rectifying waves with  $|r_L| = |t_R| = 1$  and  $t_L = r_R = 0$ .

For  $V_0 = 0$ , the scattering is both sides reflectionless when  $V_{\alpha,\beta} \neq -e^{-ik}$ . The left (right) transmission depends on  $V_{\beta(\alpha)}$ . When  $V_\alpha = V_\beta = -e^{-ik}$ , the transmission coefficients diverge with finite reflections. When  $V_\alpha = V_\beta = -e^{ik}$ , the system completely absorbs the incidence from either direction without reflection. When

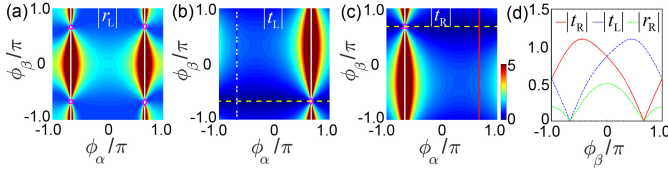


FIG. 3. Density plots of (a)  $|r_L|$ , (b)  $|t_L|$ , and (c)  $|t_R|$  as functions of  $\phi_\alpha$  and  $\phi_\beta$ .  $r_R = 0$  for  $|\phi_\alpha| \neq 2\pi/3$ ; (d)  $|t_L|$  ( $|t_R|$ ) for  $\phi_\alpha = -2\pi/3$  ( $2\pi/3$ ) and  $|r_R|$  at when  $r_L$  diverges. Solid white (dashed yellow) lines indicate the divergence (zero) at the SS. SS coincide with unity values at the marked points in (b, c). Color bars are all in (c),  $|r_L|$  and  $|t_{L,R}|$  are cut to 5. The parameters are  $V_\alpha = -e^{-i\pi/3}$ ,  $V_\beta = -e^{i\pi/3}$ ,  $V_0 = 0$ , and the incident wave vector is  $k = \pi/3$ .

$V_\alpha = -e^{-ik}$  and  $V_\beta = -e^{ik}$ , UL occurs with  $|r_L| = 1$ ,  $t_L = r_R = 0$ , and  $|t_R| \rightarrow \infty$  (square in Fig. 3).

*$\mathcal{PT}$ -symmetric side-coupled resonators.*—UPA and UL form a Hermitian conjugation pair. Their SS coincide and vanish at series connection of the two structures in a  $\mathcal{PT}$ -symmetric manner. The wave emission is absorbed and leaves finite scattering intensities.

Figure 3 depicts  $|r_{L,R}|$  and  $|t_{L,R}|$  for  $k = \pi/3$  [93].  $|\phi_{\alpha(\beta)}| = 2\pi/3$  produces a wave emission (absorption).  $|r_L| = 1$  at  $|\phi_\beta| = 2\pi/3$  and  $|r_L| \rightarrow \infty$  at  $|\phi_\alpha| = 2\pi/3$  and  $|\phi_\beta| \neq 2\pi/3$  [Fig. 3(a)].  $V_\beta = -e^{ik}$  results in  $f_0 = 0$  for the right incidence except when  $r_L$  diverges; consequently,  $r_R = 0$ . Figures 3(b) and 3(c) depict  $|t_L|$  and  $|t_R|$ .  $|t_L|$  diverges at  $\phi_\alpha = 2\pi/3$ , vanishes at  $\phi_\beta = -2\pi/3$ , and becomes unity at  $\phi_\alpha = 2\pi/3$  and  $\phi_\beta = -2\pi/3$ , where the SS of the side-coupled structures coincide. Figure 3(d) depicts the scattering coefficients at  $|\phi_\alpha| = 2\pi/3$  ( $r_L$  divergence), implied by the dash-dotted blue line [ $|t_L|$  in Fig. 3(b)] and solid red line [ $|t_R|$  in Fig. 3(c)]. At  $\phi_\alpha + \phi_\beta = 0$ , the system is  $\mathcal{PT}$ -symmetric; the scattering coefficients converge when  $\phi_\alpha = -\phi_\beta = \pm 2\pi/3$ .  $\mathcal{PT}$  symmetry ensures that the persistent wave emission from resonator  $\alpha$  is directly absorbed at resonator  $\beta$  and forms a unity transmittivity. The scattering coefficients satisfy  $|r_L| = |t_L| = |t_R| = 1$ ,  $|r_R| = 0$  and the SS vanishes. At  $\phi_\alpha = \phi_\beta = 2\pi/3$ , a persistent right-going wave emission for the left incidence and a perfect absorption for the right incidence occur:  $|r_L| = 1$ ,  $|t_L| \rightarrow \infty$ , and  $r_R = t_R = 0$ . At  $\phi_\alpha = \phi_\beta = -2\pi/3$ , a persistent left-going wave emission for the right incidence and a full reflection for the left incidence occur [93].

*Simultaneous unidirectional lasing and perfect absorption.*—UPA prevents the backward flow without affecting the forward propagation, which is a versatile building block for light manipulation. Series combination of several UPAs and ULs enables more intriguing asymmetric phenomena (Fig. 4).

Connecting a right-UPA on the left side of the two side-coupled resonators in the situation marked by the magenta circle in Fig. 3, the finite left reflection from the right two side-coupled resonators is perfectly absorbed;

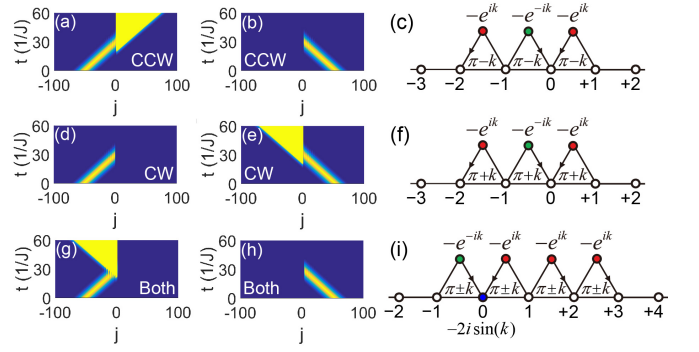


FIG. 4. Snapshots of the wave intensities and schematics of the equivalent systems for (a-f) transmissionless and (g-i) reflectionless unidirectional lasing and perfect absorption for a Gaussian wave packet of  $\sigma = 0.1$ ,  $k_c = \pi/3$ . The arrows indicate the phase directions with values inside,  $k = \pi/3$ .

consequently, a reflectionless left incident unidirectional lasing and right incident perfect absorption [Figs. 4(a) and 4(b)] is achieved in the configuration of Fig. 4(c). If all the synthetic magnetic fluxes in Fig. 4(c) are opposite, which correspond to the configuration experienced by the CW mode [Fig. 4(f)], the dynamics switch between the left and right incidences in contrast to the CCW mode [Figs. 4(d) and 4(e)]. Unidirectional lasing of different modes are toward opposite directions. Simultaneously exciting the CCW and CW modes in the left (right) side, the CCW (CW) mode induces a unidirectional lasing toward the right (left) side and the CW (CCW) mode is perfectly absorbed.

Connecting two right-UPAs on the right side of a single-direction lasing [Figs. 2(c) and 2(d)] to form the configuration shown in Fig. 4(i), the right incidence is perfectly absorbed before inducing a unidirectional lasing, resulting in a transmissionless left incident unidirectional lasing and right incident perfect absorption [Figs. 4(g) and 4(h)]. The CW mode experiences opposite synthetic magnetic fluxes, a left incident bidirectional lasing and right incident perfect absorption is realized by the left two side-coupled resonators [93] and the right two right-UPAs change into left-UPAs, which perfectly absorbing the right-going lasing. Notably, both the CCW and CW modes possess identical dynamical phenomena.

*Discussion.*—In summary, the bidirectional reflectionless as a desirable feature of UDI allows scalable combination of unidirectional dynamics, properly assembling distinct UDIs enriches the unidirectionality. The incident direction independent wave propagation is proposed, including the unidirectional lasing toward single definite direction and the one-way propagation. The simultaneous unidirectional lasing and perfect absorption is allowed. Our findings are applicable in optical waveguides [80].

The imperfections in the resonator as defects and surface roughness result in backscattering [12, 14, 100],

which induces a mode coupling and mixes the CCW and CW modes [14]. The backscattering results in mode interchanging and is unfavourable for the desirable unidirectional functionalities [102]. Directional couplers can be used to reduce the influence of backscattering [103]. As shown in the Supplementary Material [93], UPA absorbs one mode without affecting the other mode, which helps preventing the unwanted backscattering induced mode accumulation in one side; moreover, the performances of UPA, single-direction lasing, and transmissionless unidirectional lasing and perfect absorption remain good at weak backscattering. Alternatively, the backscattering is a useful resource for optical sensing [13, 28, 31].

Synthetic magnetic flux has been realized in quantum regime [58, 79, 104], it would be interesting to investigate the unidirectionality in quantum dots, cold-atoms, or trapped-ions in the frameworks of non-Hermitian physics and chiral quantum optics [55–59]. Our findings open up new directions for designing novel lasers and optical control devices including but not limited to laser, absorber, rectifier, isolator, and modulator in a variety of areas in optics and beyond.

This work was supported by NSFC (Grant No. 11605094) and Tianjin Natural Science Foundation (Grant No. 16JCYBJC40800).

---

\* jinliang@nankai.edu.cn

- [1] C. M. Bender, S. Boettcher, *Phys. Rev. Lett.* **80**, 5243 (1998).
- [2] A. Mostafazadeh, *J. Math. Phys.* **43**, 205 (2002).
- [3] H. F. Jones, *J. Phys. A* **38**, 1741 (2005).
- [4] A. Ruschhaupt, F. Delgado, and J. G. Muga, *J. Phys. A* **38**, L171 (2005).
- [5] R. El-Ganainy, K. G. Makris, D. N. Christodoulides, and Z. H. Musslimani, *Opt. Lett.* **32**, 2632 (2007).
- [6] Z. H. Musslimani, K. G. Makris, R. El-Ganainy, and D. N. Christodoulides, *Phys. Rev. Lett.* **100**, 030402 (2008).
- [7] S. Klaiman, U. Günther, and N. Moiseyev, *Phys. Rev. Lett.* **101**, 080402 (2008).
- [8] L. Jin and Z. Song, *Phys. Rev. A* **80**, 052107 (2009).
- [9] Z. Lin, H. Ramezani, T. Eichelkraut, T. Kottos, H. Cao, and D. N. Christodoulides, *Phys. Rev. Lett.* **106**, 213901 (2011).
- [10] M. Liertzer, L. Ge, A. Cerjan, A. D. Stone, H. E. Türeci, and S. Rotter, *Phys. Rev. Lett.* **108**, 173901 (2012).
- [11] D. A. Zezyulin and V. V. Konotop, *Phys. Rev. Lett.* **108**, 213906 (2012).
- [12] L. Ge and A. D. Stone, *Phys. Rev. X* **4**, 031011 (2014).
- [13] X. Zhu, H. Ramezani, C. Shi, J. Zhu, and X. Zhang, *Phys. Rev. X* **4**, 031042 (2014).
- [14] L. Chang, X. Jiang, S. Hua, C. Yang, J. Wen, L. Jiang, G. Li, G. Wang, and M. Xiao, *Nat. Photonics* **8**, 524 (2014).
- [15] H. Jing, S. K. Özdemir, X.-Y. Lü, J. Zhang, L. Yang, and F. Nori, *Phys. Rev. Lett.* **113**, 053604 (2014).
- [16] R. Fleury, D. Sounas, and A. Alù, *Nat. Commun.* **6**, 5905 (2015).
- [17] S. V. Suchkov, F. Fotsa-Ngaffo, A. Kenfack-Jiotsa, A. D. Tikeng, T. C. Kofane, Y. S. Kivshar, and A. A. Sukhorukov, *New J. Phys.* **18**, 065005 (2016).
- [18] A. Guo, G. J. Salamo, D. Duchesne, R. Morandotti, M. Volatier-Ravat, V. Aimez, G. A. Siviloglou, and D. N. Christodoulides, *Phys. Rev. Lett.* **103**, 093902 (2009).
- [19] C. E. Rüter, K. G. Makris, R. El-Ganainy, D. N. Christodoulides, M. Segev, and D. Kip, *Nat. Phys.* **6**, 192 (2010).
- [20] B. Peng, S. K. Özdemir, F. Lei, F. Monifi, M. Gianfreda, G. L. Long, S. Fan, F. Nori, C. M. Bender, and L. Yang, *Nat. Phys.* **10**, 394 (2014).
- [21] Z. Zhang, Y. Zhang, J. Sheng, L. Yang, M.-A. Miri, D. N. Christodoulides, B. He, Y. Zhang, and M. Xiao, *Phys. Rev. Lett.* **117**, 123601 (2016).
- [22] R. El-Ganainy, K. G. Makris, M. Khajavikhan, Z. H. Musslimani, S. Rotter, and D. N. Christodoulides, *Nat. Phys.* **14**, 11 (2018).
- [23] C. Dembowski, B. Dietz, H.-D. Gräf, H. L. Harney, A. Heine, W. D. Heiss, and A. Richter, *Phys. Rev. E* **69**, 056216 (2004).
- [24] H. Cartarius, J. Main, and G. Wunner, *Phys. Rev. Lett.* **99**, 173003 (2007).
- [25] M. Müller and I. Rotter, *J. Phys. A: Math. Theor.* **41**, 244018 (2008).
- [26] R. Uzdin, A. Mailybaev, and N. Moiseyev, *J. Phys. A* **44**, 435302 (2011).
- [27] W. D. Heiss, *J. Phys. A: Math. Theor.* **45**, 444016 (2012).
- [28] J. Wiersig, *Phys. Rev. Lett.* **112**, 203901 (2014).
- [29] J. Wiersig, *Phys. Rev. A* **93**, 033809 (2016).
- [30] Z.-P. Liu, J. Zhang, S. K. Özdemir, B. Peng, H. Jing, X.-Y. Lü, C.-W. Li, L. Yang, F. Nori, and Y. X. Liu, *Phys. Rev. Lett.* **117**, 110802 (2016).
- [31] W. Chen, S. K. Özdemir, G. Zhao, J. Wiersig, and L. Yang, *Nature (London)* **548**, 192 (2017).
- [32] H. Hodaiei, A. U. Hassan, S. Wittek, H. Garcia-Gracia, R. El-Ganainy, D. N. Christodoulides, and M. Khajavikhan, *Nature (London)* **548**, 187 (2017).
- [33] B. Zhen, C. W. Hsu, Y. Igarashi, L. Lu, I. Kaminer, A. Pick, S.-L. Chua, J. D. Joannopoulos, and M. Soljačić, *Nature (London)* **525**, 354 (2015).
- [34] H. Menke, M. Klett, H. Cartarius, J. Main, and G. Wunner, *Phys. Rev. A* **93**, 013401 (2016).
- [35] J. Doppler, A. A. Mailybaev, J. Böhm, U. Kuhl, A. Girschik, F. Libisch, T. J. Milburn, P. Rabl, N. Moiseyev, and S. Rotter, *Nature (London)* **537**, 76 (2016).
- [36] H. Xu, D. Mason, L. Jiang, and J. G. E. Harris, *Nature (London)* **537**, 80 (2016).
- [37] K. Ding, G. Ma, M. Xiao, Z. Q. Zhang, and C. T. Chan, *Phys. Rev. X* **6**, 021007 (2016).
- [38] A. Mostafazadeh, *Phys. Rev. Lett.* **102**, 220402 (2009).
- [39] A. Mostafazadeh, *Phys. Rev. Lett.* **110**, 260402 (2013).
- [40] Y. D. Chong, L. Ge, H. Cao, and A. D. Stone, *Phys. Rev. Lett.* **105**, 053901 (2010).
- [41] S. Longhi, *Phys. Rev. A* **82**, 031801(R) (2010).
- [42] Y. D. Chong, L. Ge, and A. D. Stone, *Phys. Rev. Lett.* **106**, 093902 (2011).
- [43] W. Wan, Y. Chong, L. Ge, H. Noh, A. D. Stone, and H. Cao, *Science* **331**, 889 (2011).
- [44] Y. Sun, W. Tan, H.-Q. Li, J. Li, and H. Chen, *Phys. Rev. Lett.* **112**, 143903 (2014).
- [45] Z. J. Wong, Y.-L. Xu, J. Kim, K. O'Brien, Y. Wang, L.



- Feng, and X. Zhang, *Nat. Photon.* **10**, 796 (2016).
- [46] C. Hang, G. Huang, and V. V. Konotop, *New J. Phys.* **18**, 085003 (2016).
- [47] L. Ge and L. Feng, *Phys. Rev. A* **95**, 013813 (2017).
- [48] D. G. Baranov, A. Krasnok, T. Shegai, A. Alù, and Y. Chong, *Nat. Rev. Mater.* **2**, 17064 (2017).
- [49] A. Regensburger, C. Bersch, M.-A. Miri, G. Onishchukov, D. N. Christodoulides, and U. Peschel, *Nature* **488**, 167 (2012).
- [50] L. Feng, Y.-L. Xu, W. S. Fegadolli, M.-H. Lu, J. E. B. Oliveira, V. R. Almeida, Y.-F. Chen, and A. Scherer, *Nat. Mater.* **12**, 108 (2013).
- [51] H. Ramezani, H.-K. Li, Y. Wang, and X. Zhang, *Phys. Rev. Lett.* **113**, 263905 (2014).
- [52] H. Ramezani, Y. Wang, E. Yablonovitch, and X. Zhang, *IEEE J. Sel. Top. Quantum Electron.* **22**, 115 (2016).
- [53] L. Jin, X. Z. Zhang, G. Zhang, and Z. Song, *Sci. Rep.* **6**, 20976 (2016).
- [54] B. Peng, S. K. Özdemir, M. Liertzer, W. Chen, J. Kramer, H. Yilmaz, J. Wiersig, S. Rotter, and Lan Yang, *Proc. Natl. Acad. Sci. USA* **113**, 6845 (2016).
- [55] T. Ramos, H. Pichler, A. J. Daley, and P. Zoller, *Phys. Rev. Lett.* **113**, 237203 (2014).
- [56] H. Pichler, T. Ramos, A. J. Daley, and P. Zoller, *Phys. Rev. A* **91**, 042116 (2015).
- [57] I. Söllner, S. Mahmoodian, S. L. Hansen, L. Midolo, A. Javadi, G. Kiršanskė, T. Pregnolato, H. El-Ella, E. H. Lee, J. D. Song, S. Stobbe, and P. Lodahl, *Nat. Nanotech.* **10**, 775 (2015).
- [58] B. Vermersch, T. Ramos, P. Hauke, and P. Zoller, *Phys. Rev. A* **93**, 063830 (2016).
- [59] P. Lodahl, S. Mahmoodian, S. Stobbe, A. Rauschenbeutel, P. Schneeweiss, J. Volz, H. Pichler, and P. Zoller, *Nature* **541**, 473 (2017).
- [60] D. Jalas, A. Petrov, M. Eich, W. Freude, S. Fan, Z. Yu, R. Baets, M. Popović, A. Melloni, J. D. Joannopoulos, M. Vanwolleghem, C. R. Doerr, and H. Renner, *Nat. Photon.* **7**, 579 (2013).
- [61] X. Yin and X. Zhang, *Nat. Mater.* **12**, 175 (2013).
- [62] J. G. Muga, J. P. Palao, B. Navarro, and I. L. Egusquiza, *Phys. Rep.* **395**, 357 (2004).
- [63] F. Cannata, J.-P. Dedonder, and A. Ventura, *Ann. Phys.* **322**, 397 (2007).
- [64] L. Bi, J. Hu, P. Jiang, D. H. Kim, G. F. Dionne, L. C. Kimerling, and C. A. Ross, *Nat. Photon.* **5**, 758 (2011).
- [65] L. Fan, J. Wang, L. T. Varghese, H. Shen, B. Niu, Y. Xuan, A. M. Weiner, and M. Qi, *Science* **335**, 447 (2012).
- [66] Z. Yu and S. Fan, *Nat. Photon.* **3**, 91 (2009).
- [67] D.-W. Wang, H.-T. Zhou, M.-J. Guo, J.-X. Zhang, J. Evers, and S.-Y. Zhu, *Phys. Rev. Lett.* **110**, 093901 (2013).
- [68] I. Shomroni, S. Rosenblum, Y. Lovsky, O. Bechler, G. Guendelman, and B. Dayan, *Science* **345**, 903 (2014).
- [69] S. Rosenblum, O. Bechler, I. Shomroni, Y. Lovsky, G. Guendelman, and B. Dayan, *Nat. Photon.* **10**, 19 (2016).
- [70] R. Fleury, D. L. Sounas, C. F. Sieck, M. R. Haberman, and A. Alù, *Science* **343**, 516 (2014).
- [71] K. Fang, Z. Yu, and S. Fan, *Nat. Photon.* **7**, 782 (2012).
- [72] L. D. Tzuang, K. Fang, P. Nussenzveig, S. Fan, and M. Lipson, *Nat. Photon.* **8**, 701 (2014).
- [73] L. Lu, J. D. Joannopoulos, and M. Soljačić, *Nat. Photon.* **8**, 821 (2014).
- [74] E. Li, B. J. Eggleton, K. Fang, and S. Fan, *Nat. Commun.* **5**, 3225 (2014).
- [75] M. Hafezi, E. A. Demler, M. D. Lukin, and J. M. Taylor, *Nat. Phys.* **7**, 907 (2011).
- [76] M. Hafezi, *Phys. Rev. Lett.* **112**, 210405 (2014).
- [77] M. Hafezi, *Int. J. Mod. Phys. B* **28**, 1441002 (2014).
- [78] S. Longhi, *Opt. Lett.* **39**, 5892 (2014).
- [79] P. Roushan, C. Neill, A. Megrant, Y. Chen, R. Babush, R. Barends, B. Campbell, Z. Chen, B. Chiaro, A. Dunsworth, A. Fowler, E. Jeffrey, J. Kelly, E. Lucero, J. Mutus, P. J. J. O'Malley, M. Neeley, C. Quintana, D. Sank, A. Vainsencher, J. Wenner, T. White, E. Kapit, H. Neven, and J. Martinis, *Nat. Phys.* **13**, 146 (2017).
- [80] S. Longhi, *Opt. Lett.* **40**, 1278 (2015).
- [81] X. Q. Li, X. Z. Zhang, G. Zhang, and Z. Song, *Phys. Rev. A* **91**, 032101 (2015).
- [82] L. Jin, P. Wang, and Z. Song, *New J. Phys.* **19**, 015010 (2017).
- [83] S. Longhi, D. Gatti, and G. Della Valle, *Phys. Rev. B* **92**, 094204 (2015).
- [84] S. Lepri and G. Casati, *Phys. Rev. Lett.* **106**, 164101 (2011).
- [85] J. D'Ambroise, P. G. Kevrekidis, and S. Lepri, *J. Phys. A: Math. Theor.* **45**, 444012 (2012).
- [86] V. V. Konotop, J. Yang, and D. A. Zezyulin, *Rev. Mod. Phys.* **88**, 035002 (2016).
- [87] H. Haken, *Laser Theory* (Springer, Berlin, 1970).
- [88] R. Roy, A. W. Yu, and S. Zhu, *Phys. Rev. Lett.* **55**, 2794 (1985).
- [89] H. P. Breuer and F. Petruccione, *The Theory of Open Quantum Systems* (Oxford University Press, Oxford, 2007).
- [90] M. O. Scully and M. S. Zubairy, *Quantum Optics* (Cambridge University Press, Cambridge, 1997).
- [91] L. Feng, Z. J. Wong, R.-M. Ma, Y. Wang, and X. Zhang, *Science* **346**, 972 (2014).
- [92] L. Jin, M. Pfender, N. Aslam, P. Neumann, S. Yang, J. Wrachtrup, and R.-B. Liu, *Nat. Commun.* **6**, 8251 (2015).
- [93] See Supplemental Material for the details on the derivation of scattering coefficients, discussions on the CCW and CW modes, and the influence of backscattering on the asymmetric dynamics.
- [94] H. A. Haus and W. P. Huang, *Proc. IEEE* **79**, 1505 (1991).
- [95] J. D. Joannopoulos, S. G. Johnson, J. N. Winn, and R. D. Meade, *Photonic Crystals: Molding the Flow of Light* (Princeton University Press, Princeton, 2008).
- [96] H. Ramezani, S. Kalish, I. Vitebskiy, and T. Kottos, *Phys. Rev. Lett.* **112**, 043904 (2014).
- [97] W. Kim, L. Covaci, and F. Marsiglio, *Phys. Rev. B* **74**, 205120 (2006).
- [98] P. Wang, L. Jin, G. Zhang, and Z. Song, *Phys. Rev. A* **94**, 053834 (2016).
- [99] T. J. Kippenberg, S. M. Spillane, and K. J. Vahala, *Opt. Lett.* **27**, 1669 (2002).
- [100] M. Borselli, T. J. Johnson, and O. Painter, *Opt. Exp.* **13**, 1515 (2005).
- [101] F. Morichetti, A. Canciamilla, C. Ferrari, M. Torregiani, A. Melloni, and M. Martinelli, *Phys. Rev. Lett.* **104**, 033902 (2010).
- [102] L. Jin and Z. Song, *Phys. Rev. A* **84**, 042116 (2011).
- [103] M. Hafezi, S. Mittal, J. Fan, A. Migdall, and J. M. Taylor, *Nat. Photon.* **7**, 1001 (2013).
- [104] N. Goldman, J. Dalibard, A. Dauphin, F. Gerbier, M. Lewenstein, P. Zoller, and I. B. Spielman, *Proc. Natl. Acad. Sci. USA* **110**, 6736 (2013).

**SUPPLEMENTARY MATERIAL FOR “INCIDENT DIRECTION INDEPENDENT WAVE  
PROPAGATION AND UNIDIRECTIONAL LASING”**

L. Jin\* and Z. Song

*School of Physics, Nankai University, Tianjin 300071, China*

**Reciprocity of scattering coefficients**

The reciprocity of transmission or reflection ( $t_L = t_R$  or  $r_L = r_R$ ) is protected by the system symmetry [1, 2]. For a scattering system of Hamiltonian  $H$ , under the notations of the parity operator  $\mathcal{P}$  and the time-reversal operator  $\mathcal{T}$ , the system is parity symmetric when  $\mathcal{P}H\mathcal{P}^{-1} = H$ , the system is time-reversal symmetric when  $\mathcal{T}H\mathcal{T}^{-1} = H$ , and the system is parity-time ( $\mathcal{PT}$ ) symmetric when  $(\mathcal{PT})H(\mathcal{PT})^{-1} = H$ . The parity symmetry leads to both reciprocal transmission and reflection ( $t_L = t_R$  and  $r_L = r_R$ ). For a system that satisfies  $\mathcal{T}H\mathcal{T}^{-1} = H^\dagger$ , the system transmission is reciprocal ( $t_L = t_R$ ); in contrast, the  $\mathcal{PT}$ -symmetry leads to symmetric transmission amplitude ( $|t_L| = |t_R|$ ).

For the Hermitian system  $H = H^\dagger$ , the time-reversal symmetry indicates  $\mathcal{T}H\mathcal{T}^{-1} = H = H^\dagger$ , thus the system transmission is reciprocal ( $t_L = t_R$ ). For the non-Hermitian system,  $\mathcal{T}H\mathcal{T}^{-1} = H^\dagger$  is satisfied in the  $\mathcal{PT}$ -symmetric systems that possessing gain/loss and the Hermitian symmetric couplings, where reciprocal transmissions ( $t_L = t_R$ ) are observed [3–5]; other  $\mathcal{PT}$ -symmetric non-Hermitian systems may satisfy  $\mathcal{T}H\mathcal{T}^{-1} = H^\dagger$ . In this Letter, the synthetic magnetic flux induced by the asymmetric coupling for unidirectional destructive interference as shown in Fig. 1(a) (Fig. 5) breaks the parity symmetry and leads to  $\mathcal{T}H\mathcal{T}^{-1} \neq H^\dagger$ , where we notice a nonreciprocal transmission ( $t_L \neq t_R$ ) from the scattering matrix  $S$  even if the system is Hermitian with real  $V_\alpha$ .

**Scattering coefficients of resonator chain with one side-coupled resonator**

The unidirectional destructive interference is valid under unequal coupling strengths between the side-coupling and the uniform coupling of the resonator chain. We consider resonator  $\alpha$  side-coupled to the uniform resonator chain as schematically illustrated in Figs. 5(a) and 5(b), and resonator 0 is on resonance with other resonators in the chain. The resonator chain has a uniform coupling  $J$ , the two side-couplings are  $g$  and  $ge^{\pm i\phi_\alpha}$ . The special case of  $g = J$  is presented in the Letter, a general case is considered here.

In the coupled-mode theory [6, 7], the equation of motion for the resonator  $j \neq -1, 0$ , and  $\alpha$  in the system illustrated in Fig. 5(a) is

$$i\frac{d\psi_j}{dt} = \omega_c\psi_j - J\psi_{j-1} - J\psi_{j+1}, \quad (15)$$

and the equations of motion for all the other resonators  $j = -1, 0$ , and  $\alpha$  are

$$i\frac{d\psi_{-1}}{dt} = \omega_c\psi_{-1} - J\psi_{-2} - J\psi_0 - g\psi_\alpha, \quad (16)$$

$$i\frac{d\psi_\alpha}{dt} = (\omega_c + V_\alpha)\psi_\alpha - g\psi_{-1} - ge^{-i\phi_\alpha}\psi_0, \quad (17)$$

$$i\frac{d\psi_0}{dt} = \omega_c\psi_0 - J\psi_{-1} - J\psi_1 - ge^{i\phi_\alpha}\psi_\alpha, \quad (18)$$

where  $\omega_c = 2\pi c/\lambda$  is the resonator frequency with  $\lambda$  the wavelength and  $c$  the light velocity in vacuum. For the dimensionless Bloch wave vector  $k$ , the dispersion relation supported by the resonator chain is  $\omega = \omega_c - 2J\cos k$  and the field amplitude is  $\psi_j = f_j e^{-i\omega t}$ . We obtain the equations of motion for the resonators  $j = -1, 0$  and  $\alpha$  at steady-state as

$$\omega f_{-1} = \omega_c f_{-1} - Jf_{-2} - Jf_0 - gf_\alpha, \quad (19)$$

$$\omega f_\alpha = (\omega_c + V_\alpha)f_\alpha - gf_{-1} - ge^{-i\phi_\alpha}f_0, \quad (20)$$

$$\omega f_0 = \omega_c f_0 - Jf_{-1} - Jf_1 - ge^{i\phi_\alpha}f_\alpha. \quad (21)$$

The steady-state wave functions are in the form of  $f_j = Ae^{ikj} + Be^{-ikj}$  ( $j < 0$ ) and  $f_j = Ce^{ikj} + De^{-ikj}$  ( $j \geq 0$ ) for the resonator  $j$  in the elastic scattering process. Thus, the wave functions of resonators  $j = 0, \pm 1, \pm 2$  are  $f_{-2} = Ae^{-2ik} + Be^{2ik}$ ,  $f_{-1} = Ae^{-ik} + Be^{ik}$ ,  $f_0 = C + D$ ,  $f_1 = Ce^{ik} + De^{-ik}$ , and  $f_2 = Ce^{2ik} + De^{-2ik}$ . Substituting

the wave functions and the dispersion relation into Eqs. (19-21), the coefficients in the steady-state wave functions satisfy

$$(-e^{-ik} - e^{ik})(Ae^{-ik} + Be^{ik}) = -(Ae^{-2ik} + Be^{2ik}) - (C + D) - \frac{g}{J}f_\alpha, \quad (22)$$

$$\left(-e^{-ik} - e^{ik} - \frac{V_\alpha}{J}\right)f_\alpha = -\frac{g}{J}(Ae^{-ik} + Be^{ik}) - \frac{g}{J}e^{-i\phi_\alpha}(C + D), \quad (23)$$

$$(-e^{-ik} - e^{ik})(C + D) = -(Ae^{-ik} + Be^{ik}) - (Ce^{ik} + De^{-ik}) - \frac{g}{J}e^{i\phi_\alpha}f_\alpha. \quad (24)$$

After eliminating  $f_\alpha$ , the coefficients satisfy

$$\left(e^{-ik} + e^{ik} + \frac{V_\alpha}{J}\right)(A + B - C - D) - \frac{g^2}{J^2}(Ae^{-ik} + Be^{ik}) - \frac{g^2}{J^2}e^{-i\phi_\alpha}(C + D) = 0, \quad (25)$$

$$(Ae^{-ik} + Be^{ik}) + e^{i\phi_\alpha}(A + B - C - D) - (Ce^{-ik} + De^{ik}) = 0. \quad (26)$$

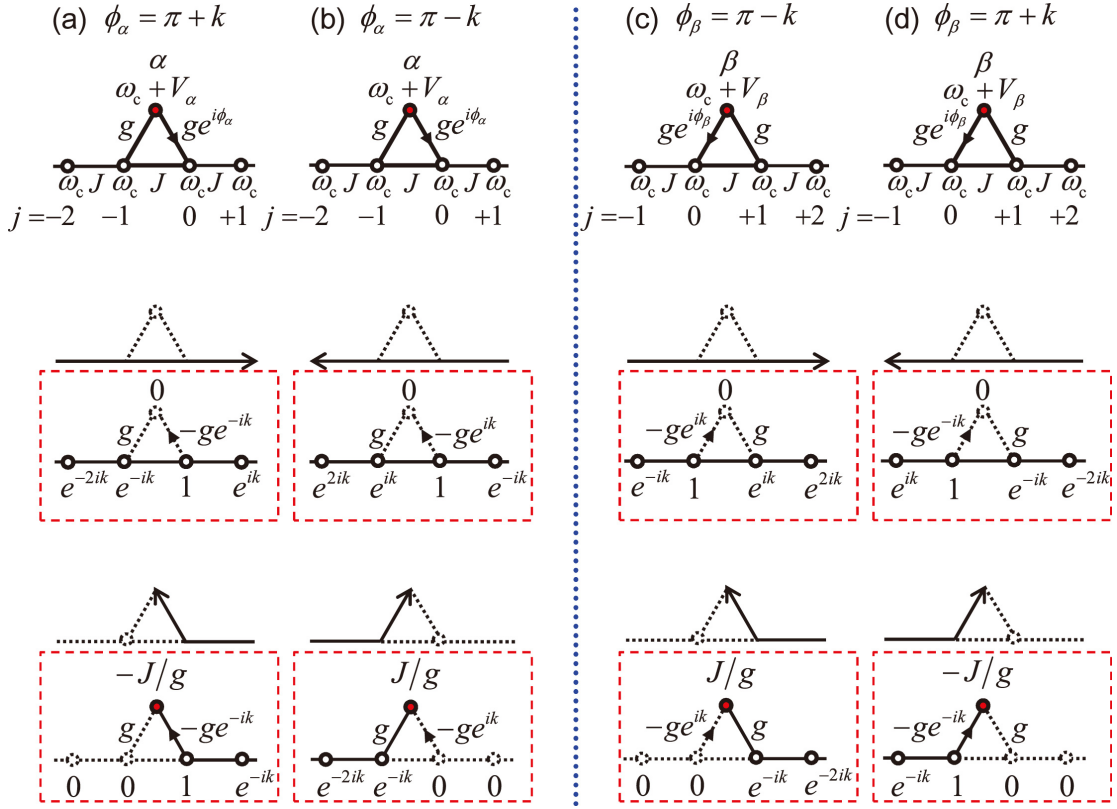


FIG. 5. Unidirectional perfect absorption. (a, c) Right-UPA. (b, d) Left-UPA. The upper panels illustrate side-coupled configurations with distinct synthetic magnetic fluxes. The values of  $\phi_\alpha$  and  $\phi_\beta$  for the unidirectional perfect absorption are marked on the top of the schematics.  $j$  is the resonator index,  $k$  is the incident wave vector, and  $V_\alpha = (g^2/J)e^{-ik} - 2J \cos k$ . The central panels illustrate the destructive interference from one incident direction and the lower panels illustrate the perfect absorption from the opposite incident direction. The wave functions and side-couplings are shown inside the red rectangles, the phase directions in the side-couplings are indicated. The dotted lines indicate the equivalently decoupled part.

As schematically illustrated in Fig. 5(a), the synthetic magnetic flux is  $\phi_\alpha = \pi + k$  [8]. Thus, equations (25, 26) reduce to

$$\left(e^{-ik} + e^{ik} + \frac{V_\alpha}{J}\right)(A + B) - \frac{g^2}{J^2}(Ae^{-ik} + Be^{ik}) - \left(e^{-ik} + e^{ik} + \frac{V_\alpha}{J} - \frac{g^2}{J^2}e^{-ik}\right)(C + D) = 0, \quad (27)$$

$$(A - C)(e^{-ik} - e^{ik}) = 0. \quad (28)$$

For the left incidence ( $D = 0$ ); substituting  $D = 0$  into Eqs. (27, 28), we obtain  $B = 0$  and  $C = A$ . Therefore,  $r_L = B/A = 0$  and  $t_L = C/A = 1$ . For the right incidence ( $A = 0$ ); substituting  $A = 0$  into Eqs. (25, 26), we obtain



$C = 0$  and

$$\left( e^{-ik} + \frac{V_\alpha}{J} + e^{ik} - \frac{g^2}{J^2} e^{ik} \right) B = \left( e^{ik} + \frac{V_\alpha}{J} + e^{-ik} - \frac{g^2}{J^2} e^{-ik} \right) D. \quad (29)$$

Therefore,  $r_R = C/D = 0$  and

$$t_R = \frac{B}{D} = \frac{J^2 e^{ik} + JV_\alpha + (J^2 - g^2) e^{-ik}}{J^2 e^{-ik} + JV_\alpha + (J^2 - g^2) e^{ik}}. \quad (30)$$

The scattering is reflectionless for the incidences from both sides. At  $g = J = 1$ , the scattering matrix [9] reduces to

$$S = \begin{pmatrix} r_L & t_R \\ t_L & r_R \end{pmatrix} = \begin{pmatrix} 0 & \frac{J^2 e^{ik} + JV_\alpha + (J^2 - g^2) e^{-ik}}{J^2 e^{-ik} + JV_\alpha + (J^2 - g^2) e^{ik}} \\ 1 & 0 \end{pmatrix} = \begin{pmatrix} 0 & \frac{e^{ik} + V_\alpha}{e^{-ik} + V_\alpha} \\ 1 & 0 \end{pmatrix}. \quad (31)$$

In Fig. 5, the steady-state wave functions are listed for the destructive interference in the middle panels and for the perfect absorption in the lower panels inside the red rectangles. The direction dependent asymmetric couplings are shown with the phase directions indicated by the arrows. The validity of steady-state wave functions can be directly checked in the equations of motion. For example, in the middle panel of Fig. 5(a), the contributions from resonators  $-1$  and  $0$  (wave functions multiple the corresponding couplings) cancel each other at resonator  $\alpha$ , leading to a completely destructive interference; thus, resonator  $\alpha$  is equivalently isolated; in the lower panel of Fig. 5(a), the left-going wave does not pass through resonator  $\alpha$ , the nonvanishing wave function of resonator  $\alpha$  results in a wave absorption and the contributions from resonators  $\alpha$  and  $0$  (wave functions multiple the corresponding couplings) cancel at resonator  $-1$ , then the left half ( $j < 0$ ) of the resonator chain is equivalently decoupled.

As schematically illustrated in Fig. 5(b), the synthetic magnetic flux is  $\phi_\alpha = \pi - k$ . Thus, equations (25, 26) reduce to

$$\left( e^{-ik} + e^{ik} + \frac{V_\alpha}{J} \right) (A + B) - \frac{g^2}{J^2} (A e^{-ik} + B e^{ik}) - \left( e^{-ik} + e^{ik} + \frac{V_\alpha}{J} - \frac{g^2}{J^2} e^{ik} \right) (C + D) = 0, \quad (32)$$

$$(B - D) (e^{ik} - e^{-ik}) = 0. \quad (33)$$

Similarly, the reflection and transmission coefficients are calculated from Eqs. (32, 33). For the left incidence ( $D = 0$ ), we obtain  $B = 0$  and

$$\left( e^{-ik} + e^{ik} + \frac{V_\alpha}{J} - \frac{g^2}{J^2} e^{ik} \right) C = \left( e^{-ik} + e^{ik} + \frac{V_\alpha}{J} - \frac{g^2}{J^2} e^{-ik} \right) A. \quad (34)$$

Therefore,  $r_L = B/A = 0$  and

$$t_L = \frac{C}{A} = \frac{J^2 e^{ik} + JV_\alpha + (J^2 - g^2) e^{-ik}}{J^2 e^{-ik} + JV_\alpha + (J^2 - g^2) e^{ik}}. \quad (35)$$

For the right incidence ( $A = 0$ ); we have  $C = 0$  and  $B = D$ . Therefore,  $r_R = C/D = 0$  and  $t_R = B/D = 1$ . At  $g = J = 1$ , the scattering matrix reduces to

$$S = \begin{pmatrix} r_L & t_R \\ t_L & r_R \end{pmatrix} = \begin{pmatrix} 0 & 1 \\ \frac{J^2 e^{ik} + JV_\alpha + (J^2 - g^2) e^{-ik}}{J^2 e^{-ik} + JV_\alpha + (J^2 - g^2) e^{ik}} & 0 \end{pmatrix} = \begin{pmatrix} 0 & 1 \\ \frac{e^{ik} + V_\alpha}{e^{-ik} + V_\alpha} & 0 \end{pmatrix}. \quad (36)$$

Figures 5(a) and 5(b) are the situations that the asymmetric coupling is on the right side of the triangular structure. Figs. 5(c) and 5(d) are the situations that the asymmetric coupling is on the left side of the triangular structure. The structures shown in Figs. 5(c) and 5(d) are the left-right mirror reflection (indicated by the blue dotted line) of that shown in Figs. 5(b) and 5(a), respectively. This can be recognized after substituting the resonator indexes  $\beta \rightarrow \alpha$  and  $j \rightarrow -j$ .

### Scattering coefficients of resonator chain with two side-coupled resonators

We consider equal coupling  $g = J = 1$  in the Letter. The equations of motion [Eqs. (2, 3, 7, 8, 9) in the Letter] at steady-state reduce to

$$\omega f_{-1} = \omega_c f_{-1} - f_{-2} - f_0 - f_\alpha, \quad (37)$$

$$\omega f_\alpha = (\omega_c + V_\alpha) f_\alpha - f_{-1} - e^{-i\phi_\alpha} f_0, \quad (38)$$

$$\omega f_0 = (\omega_c + V_0) f_0 - f_{-1} - f_1 - e^{i\phi_\alpha} f_\alpha - e^{i\phi_\beta} f_\beta, \quad (39)$$

$$\omega f_\beta = (\omega_c + V_\beta) f_\beta - f_1 - e^{-i\phi_\beta} f_0, \quad (40)$$

$$\omega f_1 = \omega_c f_1 - f_0 - f_2 - f_\beta. \quad (41)$$

The steady-state wave functions are in form of  $f_j = Ae^{ikj} + Be^{-ikj}$  ( $j < 0$ ) and  $f_j = Ce^{ikj} + De^{-ikj}$  ( $j > 0$ ) for the resonator  $j$ . Substituting the wave functions  $f_{-2} = Ae^{-2ik} + Be^{2ik}$ ,  $f_{-1} = Ae^{-ik} + Be^{ik}$ ,  $f_1 = Ce^{ik} + De^{-ik}$ ,  $f_2 = Ce^{2ik} + De^{-2ik}$ , and the dispersion relation  $\omega = \omega_c - 2 \cos k$  into Eqs. (37-41), we obtain

$$(-e^{-ik} - e^{ik})(Ae^{-ik} + Be^{ik}) = -(Ae^{-2ik} + Be^{2ik}) - f_0 - f_\alpha, \quad (42)$$

$$(-e^{-ik} - e^{ik} - V_\alpha) f_\alpha = -(Ae^{-ik} + Be^{ik}) - e^{-i\phi_\alpha} f_0, \quad (43)$$

$$(e^{-ik} - e^{ik} - V_0) f_0 = -(Ae^{-ik} + Be^{ik}) - (Ce^{ik} + De^{-ik}) - e^{i\phi_\alpha} f_\alpha - e^{i\phi_\beta} f_\beta, \quad (44)$$

$$(e^{-ik} - e^{ik} - V_\beta) f_\beta = -(Ce^{ik} + De^{-ik}) - e^{-i\phi_\beta} f_0, \quad (45)$$

$$(-e^{-ik} - e^{ik})(Ce^{ik} + De^{-ik}) = -f_0 - (Ce^{2ik} + De^{-2ik}) - f_\beta. \quad (46)$$

After simplification, we have

$$f_\alpha = A + B - f_0, \quad (47)$$

$$(e^{ik} + V_\alpha) A + (e^{-ik} + V_\alpha) B = (e^{-ik} + e^{ik} + V_\alpha + e^{-i\phi_\alpha}) f_0, \quad (48)$$

$$(e^{-ik} + e^{i\phi_\alpha}) A + (e^{ik} + e^{i\phi_\alpha}) B + (e^{ik} + e^{i\phi_\beta}) C + (e^{-ik} + e^{i\phi_\beta}) D = (e^{-ik} + e^{ik} + V_0 + e^{i\phi_\alpha} + e^{i\phi_\beta}) f_0, \quad (49)$$

$$(e^{-ik} + V_\beta) C + (e^{ik} + V_\beta) D = (e^{-ik} + e^{ik} + V_\beta + e^{-i\phi_\beta}) f_0, \quad (50)$$

$$f_\beta = C + D - f_0. \quad (51)$$

For the left incidence ( $D = 0$ ), we obtain the left reflection coefficient  $r_L = B/A$  and the left transmission coefficient  $t_L = C/A$ ,

$$r_L = \frac{(e^{ik} + V_\alpha)[(e^{i\phi_\alpha} + e^{-ik} + V_0)(e^{-ik} + V_\beta) - (e^{ik} + e^{-i\phi_\beta})(e^{i\phi_\beta} + e^{ik})] - (e^{-ik} + e^{ik} + V_\alpha + e^{-i\phi_\alpha})(e^{-ik} + V_\beta)(e^{i\phi_\alpha} + e^{-ik})}{(e^{-ik} + V_\alpha)[(e^{ik} + e^{-i\phi_\beta})(e^{i\phi_\beta} + e^{ik}) - (e^{i\phi_\alpha} + e^{-ik} + V_0)(e^{-ik} + V_\beta)] + (e^{-ik} + e^{ik} + V_\alpha + e^{-i\phi_\alpha})(e^{-ik} + V_\beta)(e^{i\phi_\alpha} + e^{ik})}, \quad (52)$$

$$t_L = \frac{(e^{-ik} + V_\beta + e^{ik} + e^{-i\phi_\beta})[(e^{ik} + V_\alpha)(e^{i\phi_\alpha} + e^{ik}) - (e^{-ik} + V_\alpha)(e^{i\phi_\alpha} + e^{-ik})]}{(e^{-ik} + V_\alpha)[(e^{ik} + e^{-i\phi_\beta})(e^{i\phi_\beta} + e^{ik}) - (e^{-ik} + V_0 + e^{i\phi_\alpha})(e^{-ik} + V_\beta)] + (e^{-ik} + e^{ik} + V_\alpha + e^{-i\phi_\alpha})(e^{-ik} + V_\beta)(e^{i\phi_\alpha} + e^{ik})}.$$

For the right incidence ( $A = 0$ ), we obtain the right reflection coefficient  $r_R = C/D$  and the right transmission coefficient  $t_R = B/D$ ,

$$r_R = \frac{(e^{ik} + V_\beta)[(e^{i\phi_\beta} + e^{-ik} + V_0)(e^{-ik} + V_\alpha) - (e^{ik} + e^{-i\phi_\alpha})(e^{ik} + e^{i\phi_\alpha})] - (e^{-ik} + e^{ik} + V_\beta + e^{-i\phi_\beta})(e^{-ik} + V_\alpha)(e^{-ik} + e^{i\phi_\beta})}{(e^{-ik} + V_\beta)[(e^{ik} + e^{-i\phi_\alpha})(e^{ik} + e^{i\phi_\alpha}) - (e^{-ik} + V_\alpha)(e^{i\phi_\beta} + e^{-ik} + V_0)] + (e^{-ik} + e^{ik} + V_\beta + e^{-i\phi_\beta})(e^{-ik} + V_\alpha)(e^{ik} + e^{i\phi_\beta})}, \quad (53)$$

$$t_R = \frac{(e^{-ik} + e^{ik} + V_\alpha + e^{-i\phi_\alpha})[(e^{ik} + e^{i\phi_\beta})(e^{ik} + V_\beta) - (e^{-ik} + e^{i\phi_\beta})(e^{-ik} + V_\beta)]}{(e^{-ik} + V_\beta)[(e^{ik} + e^{i\phi_\alpha})(e^{ik} + e^{-i\phi_\alpha}) - (e^{-ik} + V_\alpha)(e^{i\phi_\beta} + e^{-ik} + V_0)] + (e^{-ik} + e^{ik} + V_\beta + e^{-i\phi_\beta})(e^{-ik} + V_\alpha)(e^{ik} + e^{i\phi_\beta})}.$$

The interference is clear when the system is not at spectral singularities. In the case of  $e^{ik} + e^{-i\phi_\beta} = 0$ ,  $r_L$  and  $t_L$  are irrelevant to  $V_\beta$ , the side-coupled resonator  $\beta$  is isolated due to the destructive interference for the left incidence; thus, the scattering is only affected by  $V_\alpha$  and  $V_0$ . On the contrary, when  $e^{ik} + e^{-i\phi_\alpha} = 0$ , resonator  $\alpha$  is isolated for the right incidence and  $r_R$  and  $t_R$  are irrelevant to  $V_\alpha$ . When  $e^{ik} + e^{i\phi_\beta} = 0$ ,  $r_L$  and  $t_R$  are  $V_\beta$  irrelevant. This indicates that  $V_\beta$  does not affect the left-going waves (for incidence from either side). Similarly, when  $e^{ik} + e^{i\phi_\alpha} = 0$ ,  $t_L$  and  $r_R$  are  $V_\alpha$  irrelevant;  $V_\alpha$  does not affect the right-going waves (for incidence from either side). Different matches of the synthetic magnetic fluxes result in different influences of the side-coupled resonators.

In the combination of  $e^{ik} + e^{i\phi_\alpha} = 0$  and  $e^{ik} + e^{i\phi_\beta} = 0$ , e.g.,  $\phi_\alpha = \phi_\beta = \pi + k$ , the left reflection and right transmission coefficients (the left-going waves) are  $V_\beta$  irrelevant; the left transmission and right reflection coefficients

(the right-going waves) are  $V_\alpha$  irrelevant. The reflection and transmission coefficients reduce to

$$r_L = \frac{-(e^{ik} + V_\alpha) V_0}{(e^{-ik} + V_\alpha)(e^{i\phi_\alpha} + e^{-ik} + V_0)}, t_L = \frac{(e^{ik} + V_\beta)(e^{i\phi_\alpha} + e^{-ik})}{(e^{-ik} + V_0 + e^{i\phi_\alpha})(e^{-ik} + V_\beta)}, \quad (54)$$

$$r_R = \frac{-(e^{ik} + V_\beta) V_0}{(e^{-ik} + V_\beta)(e^{i\phi_\beta} + e^{-ik} + V_0)}, t_R = \frac{(e^{ik} + V_\alpha)(e^{-ik} + e^{i\phi_\beta})}{(e^{-ik} + V_\alpha)(e^{i\phi_\beta} + e^{-ik} + V_0)}. \quad (55)$$

One-way propagation occurs at  $V_\alpha = -\cos k + 3^{\pm 1} i \sin k$ ,  $V_\beta = -e^{ik}$ , and  $V_0 = -2i \sin k$ . Resonator  $\alpha$  tunes the amplitude of the left-going propagating wave; resonator  $\beta$  absorbs the right-going propagating wave. The wave is either completely left reflected or completely right transmitted, i.e.,  $|r_L| = |t_R| = 1$  and  $t_L = r_R = 0$ . Notably, the one-way propagation can be realized in another way by assembling one more side-coupled resonator. For example, assembling the unidirectional perfect absorption structure of left perfect absorption and right resonant transmission [left-UPA in Fig. 5(b) or 5(d)] on the right side of the  $\mathcal{PT}$ -symmetric two side-coupled structure in the situations of Fig. 6(a) or 6(d) in section C enables the one-way propagation. A single-direction lasing occurs at  $\phi_\alpha = \phi_\beta = \pi + k$ ,  $V_\alpha = -e^{-ik}$ ,  $V_0 = -2i \sin k$ , and  $V_\beta = -e^{ik}$ .

In the combination of  $e^{ik} + e^{-i\phi_\alpha} = 0$  and  $e^{ik} + e^{-i\phi_\beta} = 0$ , e.g.,  $\phi_\alpha = \phi_\beta = \pi - k$ , the left (right) reflection and transmission coefficients are  $V_{\beta(\alpha)}$  irrelevant. The reflection and transmission coefficients reduce to

$$r_L = \frac{(e^{ik} + V_\alpha) V_0}{(e^{-ik} + V_\alpha)(e^{i\phi_\alpha} + e^{ik} - V_0)}, t_L = \frac{(e^{ik} + V_\alpha)(e^{i\phi_\alpha} + e^{ik})}{(e^{-ik} + V_\alpha)(e^{i\phi_\alpha} + e^{ik} - V_0)}, \quad (56)$$

$$r_R = \frac{(e^{ik} + V_\beta) V_0}{(e^{-ik} + V_\beta)(e^{ik} + e^{i\phi_\beta} - V_0)}, t_R = \frac{(e^{ik} + V_\beta)(e^{ik} + e^{i\phi_\beta})}{(e^{-ik} + V_\beta)(e^{ik} + e^{i\phi_\beta} - V_0)}. \quad (57)$$

In practice, this case reveals the dynamics of the CW mode when the CCW mode experienced the synthetic magnetic fluxes  $\phi_\alpha = \phi_\beta = \pi + k$  in the system. A simultaneous left incident bidirectional lasing and right incident perfect absorption occurs at  $\phi_\alpha = \phi_\beta = \pi - k$ ,  $V_\alpha = -e^{-ik}$ ,  $V_0 = -2i \sin k$ , and  $V_\beta = -e^{ik}$ .

### Scattering coefficients of $\mathcal{PT}$ -symmetric resonator chain with two side-coupled resonators

We consider equal coupling  $g = J = 1$  in the Letter, the situation of  $\mathcal{PT}$ -symmetric resonator chain is discussed in this section. Resonator 0 is on resonance with other resonators in the chain ( $V_0 = 0$ ), the side-coupled resonators are  $\mathcal{PT}$ -symmetric,  $V_\alpha = -e^{-ik}$  and  $V_\beta = -e^{ik}$ . Substituting the wave functions  $f_{-2} = Ae^{-2ik} + Be^{2ik}$ ,  $f_{-1} = Ae^{-ik} + Be^{ik}$ ,  $f_1 = Ce^{ik} + De^{-ik}$  and  $f_2 = Ce^{2ik} + De^{-2ik}$ , and the dispersion relation  $\omega = \omega_c - 2 \cos k$  into the equations of motion at steady-state [Eqs. (37-41)], we have

$$f_\alpha = A + B - f_0, \quad (58)$$

$$(e^{ik} + e^{-ik} + V_\alpha) f_\alpha = (Ae^{-ik} + Be^{ik}) + e^{-i\phi_\alpha} f_0, \quad (59)$$

$$(e^{ik} + e^{-ik}) f_0 = (Ae^{-ik} + Be^{ik}) + (Ce^{ik} + De^{-ik}) + e^{i\phi_\alpha} f_\alpha + e^{i\phi_\beta} f_\beta, \quad (60)$$

$$(e^{ik} + e^{-ik} + V_\beta) f_\beta = (Ce^{ik} + De^{-ik}) + e^{-i\phi_\beta} f_0, \quad (61)$$

$$f_\beta = C + D - f_0, \quad (62)$$

after simplification, we obtain

$$(e^{ik} + V_\alpha) A + (e^{-ik} + V_\alpha) B = (e^{ik} + e^{-ik} + V_\alpha + e^{-i\phi_\alpha}) f_0, \quad (63)$$

$$(e^{ik} + e^{-ik} + e^{i\phi_\alpha} + e^{i\phi_\beta}) f_0 = (e^{-ik} + e^{i\phi_\alpha}) A + (e^{ik} + e^{i\phi_\alpha}) B + (e^{ik} + e^{i\phi_\beta}) C + (e^{-ik} + e^{i\phi_\beta}) D, \quad (64)$$

$$(e^{-ik} + V_\beta) C + (e^{ik} + V_\beta) D = (e^{ik} + e^{-ik} + V_\beta + e^{-i\phi_\beta}) f_0. \quad (65)$$

For the left incidence ( $D = 0$ ), we obtain  $r_L = B/A$  and  $t_L = C/A$  as

$$r_L = \frac{(e^{-ik} + e^{i\phi_\alpha}) \frac{(e^{ik} + e^{-ik} + V_\alpha + e^{-i\phi_\alpha})(e^{-ik} + V_\beta)}{(e^{ik} + e^{-ik} + V_\beta + e^{-i\phi_\beta})} - \left[ \frac{(e^{ik} + e^{-ik} + e^{i\phi_\alpha} + e^{i\phi_\beta})(e^{-ik} + V_\beta)}{(e^{ik} + e^{-ik} + V_\beta + e^{-i\phi_\beta})} - (e^{ik} + e^{i\phi_\beta}) \right] (e^{ik} + V_\alpha)}{\left[ \frac{(e^{ik} + e^{-ik} + e^{i\phi_\alpha} + e^{i\phi_\beta})(e^{-ik} + V_\beta)}{(e^{ik} + e^{-ik} + V_\beta + e^{-i\phi_\beta})} - (e^{ik} + e^{i\phi_\beta}) \right] (e^{-ik} + V_\alpha) - (e^{ik} + e^{i\phi_\alpha}) \frac{(e^{ik} + e^{-ik} + V_\alpha + e^{-i\phi_\alpha})(e^{-ik} + V_\beta)}{(e^{ik} + e^{-ik} + V_\beta + e^{-i\phi_\beta})}}, \quad (66)$$

$$t_L = \frac{\left[ (e^{-ik} + e^{i\phi_\alpha}) - (e^{ik} + e^{i\phi_\alpha}) \frac{(e^{ik} + V_\alpha)}{(e^{-ik} + V_\alpha)} \right] (e^{-ik} + V_\alpha)}{\left[ \frac{(e^{ik} + e^{-ik} + e^{i\phi_\alpha} + e^{i\phi_\beta})(e^{-ik} + V_\beta)}{(e^{ik} + e^{-ik} + V_\beta + e^{-i\phi_\beta})} - (e^{ik} + e^{i\phi_\beta}) \right] (e^{-ik} + V_\alpha) - (e^{ik} + e^{i\phi_\alpha}) \frac{(e^{ik} + e^{-ik} + V_\alpha + e^{-i\phi_\alpha})(e^{-ik} + V_\beta)}{(e^{ik} + e^{-ik} + V_\beta + e^{-i\phi_\beta})}}. \quad (67)$$

For the right incidence ( $A = 0$ ), we obtain  $r_R = C/D$  and  $t_R = B/D$  as

$$r_R = \frac{\frac{(e^{ik} + e^{-ik} + V_\beta + e^{-i\phi_\beta})(e^{-ik} + V_\alpha)}{(e^{ik} + e^{-ik} + V_\alpha + e^{-i\phi_\alpha})} (e^{-ik} + e^{i\phi_\beta}) - \left[ \frac{(e^{ik} + e^{-ik} + e^{i\phi_\alpha} + e^{i\phi_\beta})(e^{-ik} + V_\alpha)}{(e^{ik} + e^{-ik} + V_\alpha + e^{-i\phi_\alpha})} - (e^{ik} + e^{i\phi_\alpha}) \right] (e^{ik} + V_\beta)}{\left[ \frac{(e^{ik} + e^{-ik} + e^{i\phi_\alpha} + e^{i\phi_\beta})(e^{-ik} + V_\alpha)}{(e^{ik} + e^{-ik} + V_\alpha + e^{-i\phi_\alpha})} - (e^{ik} + e^{i\phi_\alpha}) \right] (e^{-ik} + V_\beta) - \frac{(e^{ik} + e^{-ik} + V_\beta + e^{-i\phi_\beta})(e^{-ik} + V_\alpha)}{(e^{ik} + e^{-ik} + V_\alpha + e^{-i\phi_\alpha})} (e^{ik} + e^{i\phi_\beta})}, \quad (68)$$

$$t_R = \frac{\left[ (e^{-ik} + e^{i\phi_\beta}) - (e^{ik} + e^{i\phi_\beta}) \frac{(e^{ik} + V_\beta)}{(e^{-ik} + V_\beta)} \right] (e^{-ik} + V_\beta)}{\left[ \frac{(e^{ik} + e^{-ik} + e^{i\phi_\alpha} + e^{i\phi_\beta})(e^{-ik} + V_\alpha)}{(e^{ik} + e^{-ik} + V_\alpha + e^{-i\phi_\alpha})} - (e^{ik} + e^{i\phi_\alpha}) \right] (e^{-ik} + V_\beta) - \frac{(e^{ik} + e^{-ik} + V_\beta + e^{-i\phi_\beta})(e^{-ik} + V_\alpha)}{(e^{ik} + e^{-ik} + V_\alpha + e^{-i\phi_\alpha})} (e^{ik} + e^{i\phi_\beta})}. \quad (69)$$

After substituting  $V_\alpha = -e^{-ik}$  and  $V_\beta = -e^{ik}$  into the expressions, we obtain the scattering coefficients  $r_L$ ,  $t_L$ ,  $r_R$ , and  $t_R$  after simplification.

The left reflection coefficient  $r_L$  diverges at  $\phi_\alpha = \pi \pm k$  when  $\phi_\beta \neq \pi \pm k$ . At  $r_L$  divergence of  $\phi_\alpha = \pi + k$ , we obtain  $t_R \rightarrow \infty$  and

$$t_L = -\frac{(e^{ik} - e^{-ik})^2 (e^{-ik} + e^{-i\phi_\beta})}{2(\cos k + \cos \phi_\beta - 4i \sin^3 k)}, \quad (70)$$

$$r_R = \frac{e^{-2ik} (\cos \phi_\beta + \cos k)}{\cos \phi_\beta + \cos k - 4i \sin^3 k}. \quad (71)$$

At  $r_L$  divergence of  $\phi_\alpha = \pi - k$ , we obtain  $t_L \rightarrow \infty$  and

$$t_R = -\frac{(e^{ik} - e^{-ik})^2 (e^{-ik} + e^{i\phi_\beta})}{2(\cos k + \cos \phi_\beta - 4i \sin^3 k)}, \quad (72)$$

$$r_R = \frac{e^{-2ik} (\cos \phi_\beta + \cos k)}{\cos \phi_\beta + \cos k - 4i \sin^3 k}. \quad (73)$$

Notice that  $r_R$  are identical for  $r_L$  divergence at  $\phi_\alpha = \pi \pm k$ .

For  $\phi_\alpha = \pi \pm k$  and  $\phi_\beta = \pi \pm k$ . The scattering coefficients  $\{r_L, t_L, r_R, t_R\}$  are  $\{-1, 1, 0, -1\}$  at (a)  $\phi_\alpha = \pi + k, \phi_\beta = \pi - k$ ;  $\{-1, \infty, 0, 0\}$  at (b)  $\phi_\alpha = \pi - k, \phi_\beta = \pi - k$ ;  $\{-1, 0, 0, \infty\}$  at (c)  $\phi_\alpha = \pi + k, \phi_\beta = \pi + k$ ; and  $\{-1, -1, 0, 1\}$  at (d)  $\phi_\alpha = \pi - k, \phi_\beta = \pi + k$ . The dynamics are illustrated in Fig. 6.

We can also directly substitute  $V_\alpha = -e^{-ik}$  and  $V_\beta = -e^{ik}$  into the equations of motion at steady-state [Eqs. (37-41)], the calculation of the scattering coefficients is more concise (however, the scattering coefficients at  $r_L$  divergence can not be obtained in this way). We can obtain

$$f_\alpha = A + B - f_0, \quad (74)$$

$$e^{ik} f_\alpha = (Ae^{-ik} + Be^{ik}) + e^{-i\phi_\alpha} f_0, \quad (75)$$

$$(e^{ik} + e^{-ik}) f_0 = (Ae^{-ik} + Be^{ik}) + (Ce^{ik} + De^{-ik}) + e^{i\phi_\alpha} f_\alpha + e^{i\phi_\beta} f_\beta, \quad (76)$$

$$e^{-ik} f_\beta = (Ce^{ik} + De^{-ik}) + e^{-i\phi_\beta} f_0, \quad (77)$$

$$f_\beta = C + D - f_0, \quad (78)$$

then, the scattering coefficients when  $r_L$  does not diverge ( $\phi_\alpha \neq \pi \pm k$ ) can be calculated as follows. For the left incidence ( $D = 0$ ), we obtain

$$r_L = \frac{B}{A} = \frac{(e^{ik} + e^{i\phi_\beta}) (e^{ik} + e^{-i\phi_\beta}) - (e^{-ik} + e^{i\phi_\alpha}) (e^{-ik} + e^{-i\phi_\alpha})}{(e^{i\phi_\alpha} + e^{ik}) (e^{-i\phi_\alpha} + e^{ik})}, \quad (79)$$

$$t_L = \frac{C}{A} = -\frac{e^{-i\phi_\beta} + e^{-ik}}{e^{-i\phi_\alpha} + e^{ik}}. \quad (80)$$

For the right incidence ( $A = 0$ ), we obtain

$$r_R = \frac{C}{D} = 0, \quad (81)$$

$$t_R = \frac{B}{D} = -\frac{e^{i\phi_\beta} + e^{-ik}}{e^{i\phi_\alpha} + e^{ik}}. \quad (82)$$

The coefficients acquired are in accord with Eqs. (66-69).

We perform the time evolution of a Gaussian wave packet to demonstrate the scattering dynamics, the uniformly coupled resonator chain is cut at the resonators  $-100$  and  $100$ . The Gaussian wave packet used in the simulations is

$$|\Psi(0, j)\rangle = (\sqrt{\pi}/\sigma)^{-1/2} \sum_j e^{-(\sigma^2/2)(j-N_c)^2} e^{ik_c j} |j\rangle, \quad (83)$$

centered at  $N_c$  with wave vector  $k_c$ , and  $\sigma$  characterizes its width.  $j$  is the resonator index and  $|j\rangle$  is the basis of the resonator chain.

The dynamics at special cases of  $|\phi_\alpha| = 2\pi/3$  and  $|\phi_\beta| = 2\pi/3$  are depicted in Fig. 6. Synthetic magnetic flux at  $\phi_\alpha = -2\pi/3$  ( $2\pi/3$ ) produces a left-going (right-going) wave emission [Fig. 7]; synthetic magnetic flux at  $\phi_\beta = -2\pi/3$  ( $2\pi/3$ ) realizes a right-going (left-going) wave absorption [Fig. 5]. In Figs. 6(a) and 6(d), the whole scattering system is  $\mathcal{PT}$ -symmetric. The unidirectional spectral singularities for wave emission and wave absorption coincide.  $\mathcal{PT}$  symmetry ensures that the persistently emitted waves from resonator  $\alpha$  are directly absorbed at resonator  $\beta$  and form a unity transmittivity. The transmittivity is symmetric  $|t_L|^2 = |t_R|^2 = 1$ , and the spectral singularities vanish. The snapshots presented in Figs. 6(a) and 6(d) are similar: the transmittivity and reflectivity for the left incidence are both unity; the transmittivity is unity and reflectivity is zero for the right incidence. However, the modal amplitude diverges at resonator 0 when  $\phi_\alpha = 2\pi/3$  and  $\phi_\beta = -2\pi/3$ , which is imprinted from the bright line at resonator 0 after scattering in Fig. 6(d). In addition, the difference of the synthetic magnetic fluxes results in a relative phase difference  $\pi$  for the transmitted waves after scattering between the left and right incidences; however, the reflection coefficients have the same phase. One-way propagation is again realized through assembling one more side-coupled resonator. Connecting a unidirectional perfect absorption structure of left perfect absorption and right resonant transmission [left-UPA in Fig. 5(b) or 5(d)] on the right side of the  $\mathcal{PT}$ -symmetric two side-coupled resonators at the situation shown in Fig. 6(a) or 6(d), the one-way propagation is realized as mentioned in section B.

Figure 6(b) illustrates a persistent right-going wave emission (unidirectional lasing) for a left incidence and perfect absorption for a right incidence. Additional unidirectional perfect absorption structure of right perfect absorption and left resonant transmission [right-UPA in Fig. 5(a) or 5(c)] on the left side of the two side-coupled resonators absorbs the left-going waves; therefore, the unity left reflection is perfectly absorbed, and the reflectionless left incident unidirectional lasing and right incident perfect absorption is created as shown in Figs. 4(a) and 4(b) in the Letter. The persistent wave emissions are characterized by a Gaussian error function [10].

Figure 6(c) illustrates a persistent left-going wave emission for a right incidence and a full reflection for a left

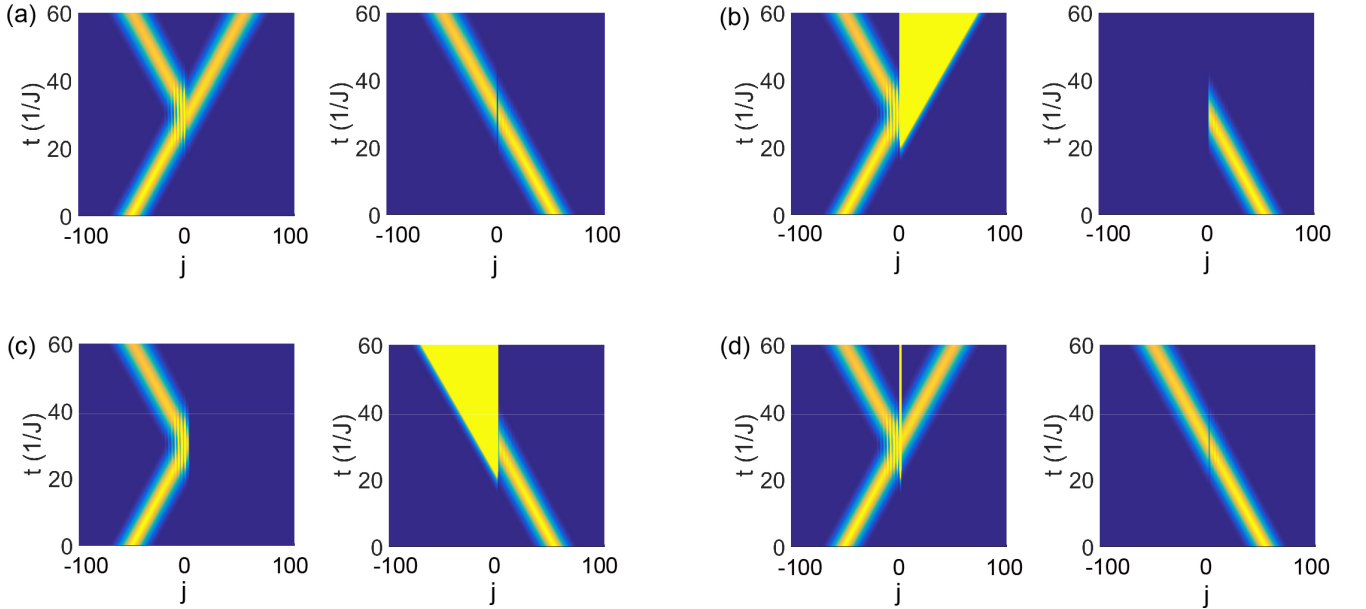


FIG. 6. Snapshots of the Gaussian wave packet dynamics for the left and right incidences at (a)  $\phi_\alpha = -\phi_\beta = -2\pi/3$ , (b)  $\phi_\alpha = \phi_\beta = 2\pi/3$ , (c)  $\phi_\alpha = \phi_\beta = -2\pi/3$ , and (d)  $\phi_\alpha = -\phi_\beta = 2\pi/3$ . They correspond to the triangle, circle, square, and diamond marked in Fig. 3(a) in the Letter. The parameters are  $V_\alpha = -e^{-i\pi/3}$ ,  $V_\beta = -e^{i\pi/3}$ , and  $V_0 = 0$ . The Gaussian wave packet with  $\sigma = 0.1$  has wave vector  $k_c = \pi/3$  in the simulations.  $||\Psi(t, j)||^2$  is depicted.

incidence; therefore, additional unidirectional perfect absorption structure of left perfect absorption and right resonant transmission [left-UPA in Fig. 5(b) or 5(d)] on the left side of the two side-coupled resonators absorbs the left incidence, and the reflectionless right incident unidirectional lasing and left incident perfect absorption is created as shown in Figs. 4(d) and 4(e) in the Letter.

The scattering coefficients  $r_{L,R}$   $t_{L,R}$  virtually share identical denominator, but their numerators are distinct. The system is at spectral singularities when the denominator goes to zero, provided that the numerator does not vanish. When the denominator and the numerator vanish simultaneously, the coefficients are obtained by calculating the limitation of expressions as wave vector  $k$  approaches the divergent wave vector. The transmission and reflection coefficients do not diverge and the spectral singularities vanish.

### Left bidirectional lasing and right perfect absorption

The influences of the side-coupled resonators  $\alpha$ ,  $\beta$  vary as the synthetic magnetic fluxes at different matches. To demonstrate the phenomenon of bidirectional lasing from one side and perfect absorption from the other side, we first show the unidirectional lasing performed in a Hermitian conjugation system of the unidirectional perfect absorption illustrated in Figs. 5(a) and 5(b). The dynamics for the left and right incidences are depicted in Figs. 7(a) and 7(b), respectively. The schematics of the Hermitian conjugation systems of unidirectional perfect absorption are illustrated in Fig. 7(c). Notice that the unidirectional lasing is toward opposite directions for the opposite incidences.

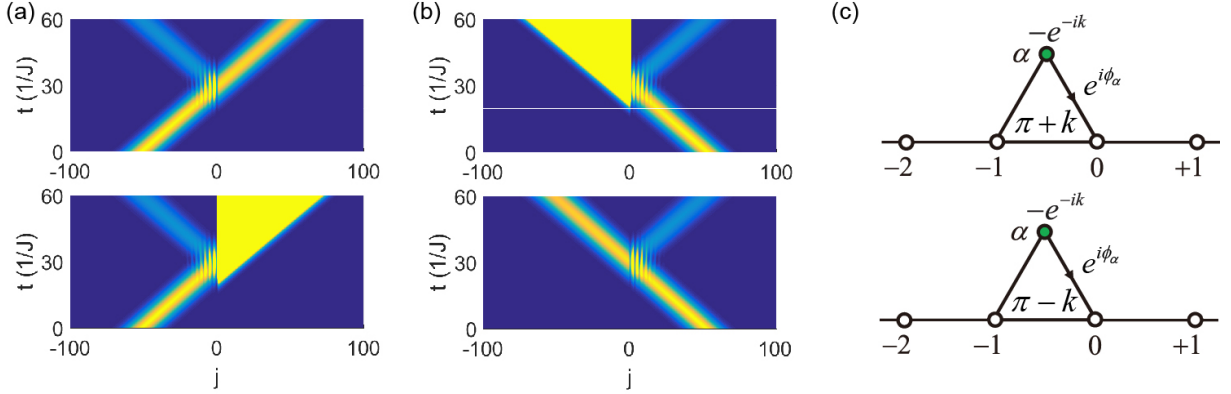


FIG. 7. (a, b) Snapshots of the Gaussian wave packet dynamics of a unidirectional lasing at  $\phi_\alpha = -2\pi/3$  and  $\phi_\alpha = 2\pi/3$  for the upper and lower panels, respectively. (c) Schematic of the system with parameters  $V_\alpha = -e^{-i\pi/3}$ ,  $k = \pi/3$ . The Gaussian wave packet with  $\sigma = 0.1$  has wave vector  $k_c = \pi/3$  in the simulations.  $|\Psi(t, j)|^2$  is depicted.

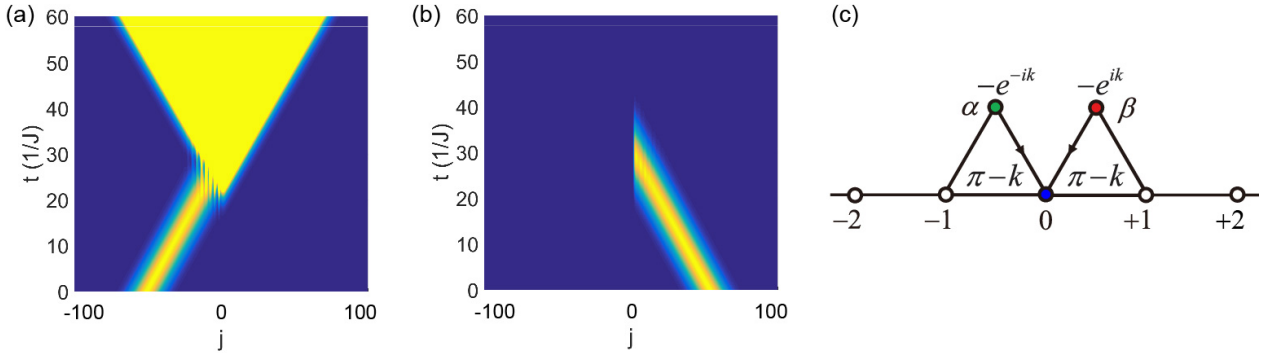


FIG. 8. Snapshots of the Gaussian wave packet dynamics for the (a) left and (b) right incidences at  $\phi_\alpha = \phi_\beta = 2\pi/3$ . (c) Schematic of the system with parameters  $V_\alpha = -e^{-i\pi/3}$ ,  $V_\beta = -e^{i\pi/3}$ , and  $V_0 = -2i \sin(\pi/3)$ ,  $k = \pi/3$ . The Gaussian wave packet with  $\sigma = 0.1$  has wave vector  $k_c = \pi/3$  in the simulations.  $|\Psi(t, j)|^2$  is depicted.



In Fig. 8, the chosen synthetic magnetic fluxes are opposite as the situation of a single-direction lasing for the CCW mode [Figs. 2(c) and 2(d) in the Letter], and other system parameters are unchanged. That is  $\phi_\alpha = \phi_\beta = \pi - k$ ,  $V_\alpha = -e^{-ik}$ ,  $V_0 = -2i \sin k$ , and  $V_\beta = -e^{ik}$ ; these characterize the CW mode in the system when the CCW mode is at single-direction lasing. The phenomenon of bidirectional lasing for incidence from one direction and perfect absorption for incidence from the other direction is simulated for a Gaussian wave packet excitation. For a left incidence, a right-going unidirectional lasing is generated at the gain resonator  $\alpha$  [lower panel of Fig. 7(a)]; which is scattered at resonator 0 with half reflected and half transmitted. The half reflected unidirectional lasing passes through resonator  $\alpha$  from the right side with unity transmittivity [lower panel of Fig. 7(b)] and forms the left-going wave emission; the half transmitted unidirectional lasing resonantly passes through resonator  $\beta$  from its left side and forms the right-going wave emission; therefore, a symmetric bidirectional lasing is created for the left incidence. For a right incidence, the Gaussian wave packet is perfectly absorbed without reflection. At  $\phi_\alpha = \phi_\beta = \pi - k$ ,  $V_\alpha = -e^{-ik}$ , and  $V_\beta = -e^{ik}$ , the bidirectional lasing for the left incidence is tuned by  $V_0$  and becomes unidirectional at  $V_0 = 0$  as depicted in Fig. 6(b).

### Wave propagation dynamics in the presence of backscattering

The surface roughness and defects in the resonator induce backscattering between the CCW and CW modes [11–13], which results in a mode coupling and an intensity interchange between two modes. For the unidirectional perfect absorption structure in Fig. 5(a), the equations of motion in the presence of backscattering for the resonators  $j < -1$  and  $j > 0$  in the chain are revised to

$$i \frac{d\psi_{CCW,j}}{dt} = \omega_c \psi_{CCW,j} - J\psi_{CCW,j-1} - J\psi_{CCW,j+1} - \kappa_j \psi_{CW,j}, \quad (84)$$

and

$$i \frac{d\psi_{CW,j}}{dt} = \omega_c \psi_{CW,j} - J\psi_{CW,j-1} - J\psi_{CW,j+1} - \kappa_j \psi_{CCW,j}, \quad (85)$$

where  $\psi_{CCW,j}$  and  $\psi_{CW,j}$  are the mode amplitudes of the CCW and CW modes in the resonator  $j$ , respectively. The coupling between the CCW and CW modes of the resonator  $j$  is  $\kappa_j$  [14]. The equations of motion for other resonators  $j = -1, 0$ , and  $\alpha$  are

$$i \frac{d\psi_{CCW,-1}}{dt} = \omega_c \psi_{CCW,-1} - J\psi_{CCW,-2} - J\psi_{CCW,0} - g\psi_{CCW,\alpha} - \kappa_{-1} \psi_{CW,-1}, \quad (86)$$

$$i \frac{d\psi_{CCW,\alpha}}{dt} = (\omega_c + V_\alpha) \psi_{CCW,\alpha} - gJ\psi_{CCW,-1} - ge^{-i\phi_\alpha} \psi_{CCW,0} - \kappa_\alpha \psi_{CW,\alpha}, \quad (87)$$

$$i \frac{d\psi_{CCW,0}}{dt} = \omega_c \psi_{CCW,0} - J\psi_{CCW,-1} - J\psi_{CCW,1} - ge^{i\phi_\alpha} \psi_{CCW,\alpha} - \kappa_0 \psi_{CW,0}, \quad (88)$$

and

$$i \frac{d\psi_{CW,-1}}{dt} = \omega_c \psi_{CW,-1} - J\psi_{CW,-2} - J\psi_{CW,0} - g\psi_{CW,\alpha} - \kappa_{-1} \psi_{CCW,-1}, \quad (89)$$

$$i \frac{d\psi_{CW,\alpha}}{dt} = (\omega_c + V_\alpha) \psi_{CW,\alpha} - gJ\psi_{CW,-1} - ge^{-i\phi_\alpha} \psi_{CW,0} - \kappa_\alpha \psi_{CCW,\alpha}, \quad (90)$$

$$i \frac{d\psi_{CW,0}}{dt} = \omega_c \psi_{CW,0} - J\psi_{CW,-1} - J\psi_{CW,1} - ge^{i\phi_\alpha} \psi_{CW,\alpha} - \kappa_0 \psi_{CCW,0}. \quad (91)$$

In the simulations shown below, the side-coupling is set  $g = J = 1$  as that in the Letter. The time evolution intensity  $|\Psi(t, j)|^2$  of an initial Gaussian excitation  $|\Psi(0, j)\rangle = (\sqrt{\pi}/\sigma)^{-1/2} \sum_j e^{-(\sigma^2/2)(j-N_c)^2} e^{ik_c j} |j\rangle$  is depicted,  $\sigma$  characterizes its width. The initial Gaussian wave packet CCW mode excitation is centered at  $N_c$  with wave vector  $k_c$ , the velocity of the Gaussian wave packet is  $2J \sin(k_c)$ . The mode coupling between the CCW and CW modes results in an intensity interchange between these two modes in the wave propagation process, which can be characterized by an intensity breathing [15].

In Figs. 9(a) and 9(b), the dynamics of a unidirectional perfect absorption are depicted in the presence of backscattering. Schematic of an equivalent configuration is shown in Fig. 9(c). At weak mode coupling ( $0 \leq \kappa_j \leq 0.01J$ ), the unidirectional perfect absorption performed for the CCW mode excitation remains good.

In Figs. 9(d) and 9(e), the coupling between the CCW and CW modes in each resonator is randomly chosen within the region  $0 \leq \kappa_j \leq 0.1J$ . A deviation from an ideal unidirectional perfect absorption is noticed. For a left incident

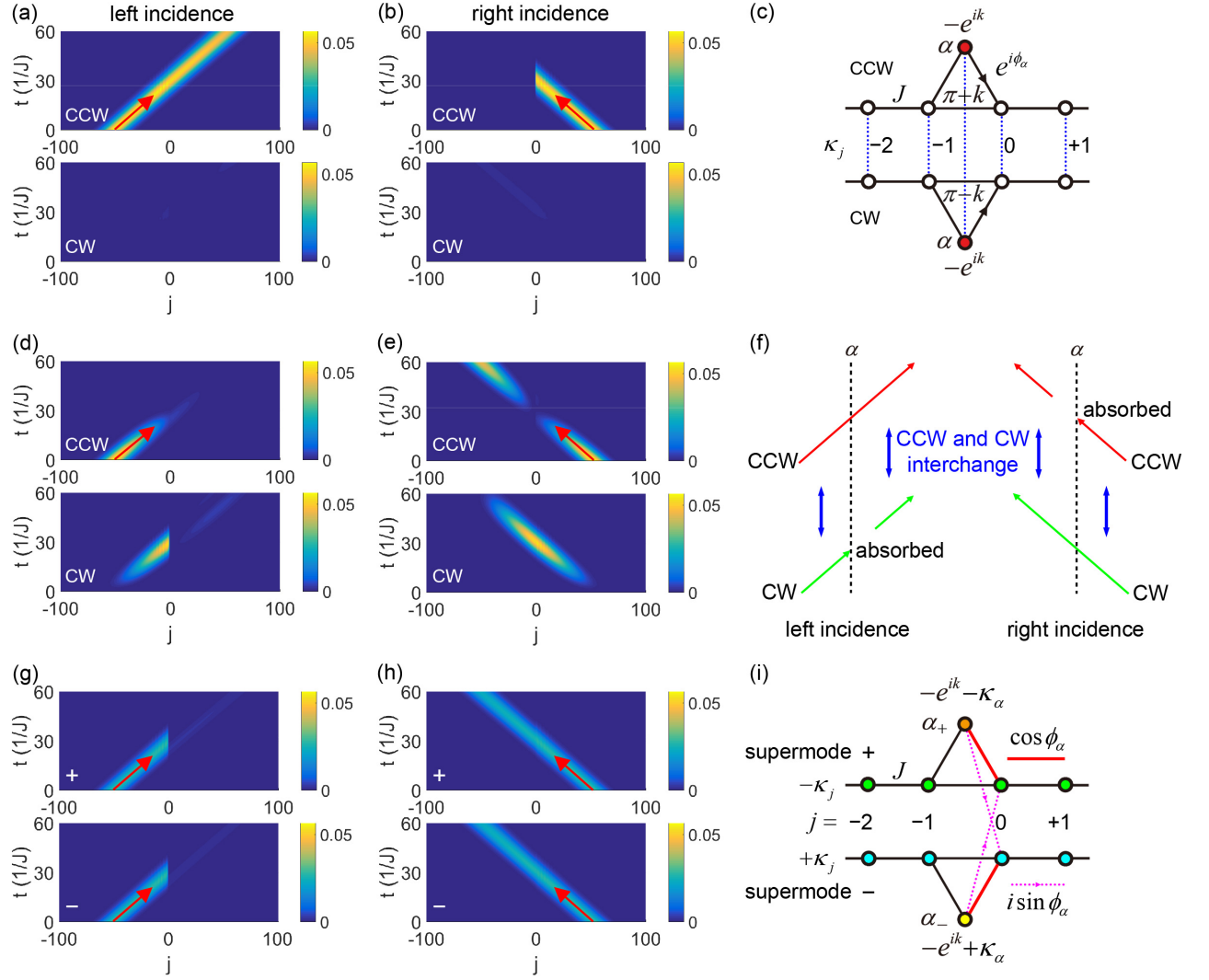


FIG. 9. (a, b, d, e) Snapshots of the intensity of a unidirectional perfect absorption. The upper (lower) panels are for the CCW (CW) mode. The initial excitation is the CCW mode Gaussian wave packet with  $\sigma = 0.1$  and wave vector  $k_c = \pi/3$ . The red arrows indicate the incidences. (c) Schematic of the system in the presence of backscattering, the coupling between the CCW and CW modes is indicated by the dotted blue lines. The system parameters are marked,  $V_\alpha = -e^{-ik}$ ,  $k = \pi/3$ . The phase direction of the coupling is indicated by the arrows in the triangular structures, the values of opposite synthetic magnetic fluxes experienced by the CCW and CW modes are marked. (f) Cartoon of the wave propagation in the presence of backscattering. (g, h) Snapshots of the intensity of a supermode unidirectional perfect absorption, the parameters are identical with that in (d, e). The upper (lower) panels are for the symmetric (antisymmetric) supermode + (-). (i) Schematic of the system in the supermode basis,  $\phi_\alpha = \pi + k$ . The green (cyan) circles indicate the symmetric (antisymmetric) supermode basis with frequency  $\omega_c - \kappa_j$  ( $\omega_c + \kappa_j$ ). In the simulations, each  $\kappa_j$  is randomly chosen within  $[0, 0.01J]$  in (a, b), within  $[0, 0.1J]$  in (d, e, g, h), and  $J = 1$ ; the wave propagation dynamics are averaged over  $10^3$  sample systems. Notice that the initial intensities in both the upper and lower panels of (g, h) are half that in the upper panels of (a, b).

CCW mode excitation [Fig. 9(d)], a CW mode Gaussian wave packet is formed with an identical velocity of the CCW mode when it propagates toward resonator  $\alpha$ ; the CCW mode wave packet resonantly transmits at resonator  $\alpha$ , but the CW mode wave packet is perfectly absorbed as predicted by Eq. (31). After the CCW mode wave packet resonantly passing through resonator  $\alpha$ , the CW mode is formed once again through the mode coupling (i.e., mode intensity breathing). Similarly, for a right incident CCW mode excitation [Fig. 9(e)], the incident left-going CCW mode wave packet is perfectly absorbed at resonator  $\alpha$ ; the backscattering induced CW mode wave packet resonantly passes through resonator  $\alpha$  from the right side to the left side, which transfers into the CCW mode after scattering. These dynamical processes are schematically illustrated in Fig. 9(f), where the red arrows represent the CCW mode

excitations, the blue double-arrows represent the interchange between the CCW and CW modes, and the green arrows represent the CW mode formed through mode coupling in the wave propagation process of the CCW mode excitation.

The mode coupling  $\kappa_j$  mixes the CCW and CW modes in the resonator  $j$ , results in the frequency shift and mode splitting [13], and creates symmetric and antisymmetric supermodes  $|j, \pm\rangle = (|j, \text{CCW}\rangle \pm |j, \text{CW}\rangle)/\sqrt{2}$  with resonant frequencies  $\omega_c \mp \kappa_j$  [14], respectively. Fig. 9(i) is a schematic of the unidirectional perfect absorption structure of Fig. 9(c) after applied a uniform transformation, the new basis is the supermodes instead of the CCW and CW modes. The supermode splitting  $2\kappa$  (if assuming a constant mode coupling  $\kappa = \kappa_j$ ) indicates that the mode coupling induced intensity breathing has a period of  $T = \pi/\kappa$  [15]. We can roughly estimate the condition of obtaining a good performance unidirectional perfect absorption, which is approximately

$$N_c/[J \sin(k_c)] \ll T. \quad (92)$$

For  $k_c = \pi/3$  and  $N_c = 50$ , we have  $\kappa \ll \pi J \sin(k_c)/N_c \approx 0.05J$ . Notice that the parameters in Figs. 9(a) and 9(b) satisfy this condition.

The intensities of the CCW and CW modes  $|\Psi(t, j)\rangle_{\text{CCW}}|^2$ ,  $|\Psi(t, j)\rangle_{\text{CW}}|^2$  are depicted in Figs. 9(d) and 9(e), notice that the breathing period approaches the propagating time ( $T \approx 63/J$  and  $N_c/[J \sin(k_c)] \approx 58/J$ ). Correspondingly, the intensities of the supermodes  $|\Psi(t, j)\rangle_{\text{CCW}} \pm |\Psi(t, j)\rangle_{\text{CW}}/\sqrt{2}|^2$  are depicted in Figs. 9(g) and 9(h). An interesting phenomenon occurs in this situation: both the symmetric and antisymmetric supermodes are left incident perfect absorption and right incident resonant transmission. This is a consequence of the proper match of the mode coupling and the wave propagating time and can be understood as follows. In Fig. 9(d), it is noticed that when the CCW mode wave packet reaches resonator  $\alpha$ , it is completely changed into the CW mode due to the proper match of mode interchange and the wave packet propagating time; then the CW mode is perfectly absorbed at resonator  $\alpha$ . The UPA absorbs the CW mode without affecting the CCW mode, which helps preventing the unwanted backscattering induced CW mode accumulation in the left side. This results in the left perfect absorption for both the symmetric and antisymmetric supermodes as shown in Fig. 9(g). The right incident CCW mode is completely changed into the CW mode when the wave packet reaches resonator  $\alpha$ , and then escapes from being absorbed; the CW mode formed resonantly passes through resonator  $\alpha$  and then changes back into the CCW mode as shown in Fig. 9(e). In this process, the right incident CCW mode is almost not affected by resonator  $\alpha$ ; therefore, both the symmetric and antisymmetric mode incidences resonantly transmit at resonator  $\alpha$  as shown in Fig. 9(h). Here, the unidirectional perfect absorber acts similarly as an isolator for the supermodes.

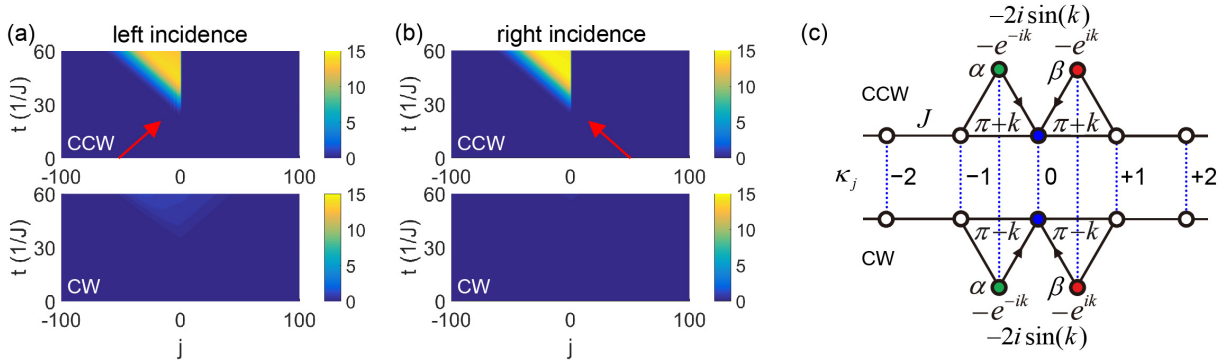


FIG. 10. (a, b) Snapshots of the intensity of a single-direction lasing. The upper (lower) panels are for the CCW (CW) mode. The initial excitation is the CCW mode Gaussian wave packet with  $\sigma = 0.1$  and wave vector  $k_c = \pi/3$ . The red arrows indicate the incidences. (c) Schematic of the system in the presence of backscattering, the coupling between the CCW and CW modes is indicated by the dotted blue lines. The system parameters are marked,  $k = \pi/3$ . The coupling phase direction is indicated by the arrows in the triangular structures, which reflect the opposite synthetic magnetic fluxes that experienced by the CCW and CW modes. In the simulations, each  $\kappa_j$  is randomly chosen within  $[0, 0.01J]$ ,  $J = 1$ ; the wave propagation dynamics are averaged over  $10^3$  sample systems.

In the presence of backscattering, the equations of motion for the systems with more side-coupled resonators are similarly extended with an additional term characterizing the coupling between the CCW and CW modes in each equation. In Figs. 10(a) and 10(b), the dynamics of a single-direction lasing for the CCW mode excitation is performed at weak mode coupling ( $0 \leq \kappa_j \leq 0.01J$ ). Schematic of an equivalent configuration is shown in Fig. 10(c). Notably, the single-direction lasing depicted in the simulation remains good. The CW mode, formed in the wave propagation process due to the mode coupling, induces a weak bidirectional lasing (Fig. 8) in the lower panel of Fig. 10(a) for the

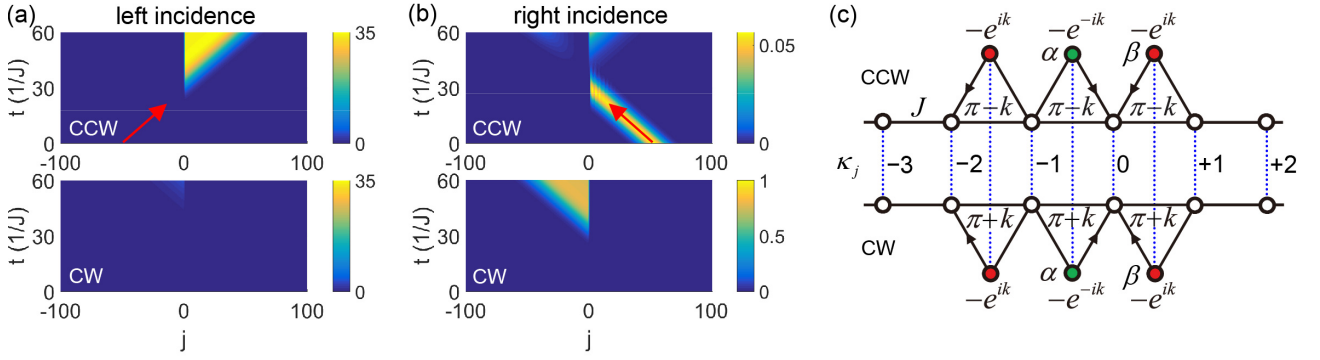


FIG. 11. Snapshots of the intensity of a reflectionless unidirectional lasing and perfect absorption for the incidences from the (a) left and (b) right. The upper (lower) panels are for the CCW (CW) mode. The initial excitation is the CCW mode Gaussian wave packet with  $\sigma = 0.1$  and wave vector  $k_c = \pi/3$ . The red arrows indicate the incidences. (c) Schematic of the system in the presence of backscattering, the coupling between the CCW and CW modes is indicated by the dotted blue lines. The system parameters are marked, where  $k = \pi/3$ . The coupling phase direction is indicated by the arrows in the triangular structures, indicating the opposite synthetic magnetic fluxes that experienced by the CCW and CW modes. In the simulations, each  $\kappa_j$  is randomly chosen within  $[0, 0.01J]$ ,  $J = 1$ ; the wave propagation dynamics are averaged over  $10^3$  sample systems.

left incident CCW mode excitation, and the CW mode formed in the wave propagation process is perfectly absorbed for the right incident CCW mode excitation as shown in the lower panel of Fig. 10(b).

In Figs. 11(a) and 11(b), the dynamics of a reflectionless unidirectional lasing and perfect absorption is performed at weak mode coupling. Schematic of an equivalent configuration is shown in Fig. 11(c). An ideal reflectionless unidirectional lasing and perfect absorption is depicted in Figs. 4(a-f) of the Letter: a left incident reflectionless transmission divergence ( $r_L = 0, t_L \rightarrow \infty$ ) and a right incident perfect absorption ( $r_R = t_R = 0$ ) for the CCW mode incidence, and a left incident perfect absorption ( $r_L = t_L = 0$ ) and a right incident reflectionless transmission divergence ( $r_R = 0, t_R \rightarrow \infty$ ) for the CW mode incidence. Notably, the reflectionless unidirectional lasing and perfect absorption is severely affected by the backscattering. This is because that the mode coupling induced weak CW mode is amplified at the gain resonator after scattering, which is not properly absorbed at the dissipative resonators due to the mode coupling; in particular, a weak left-going CW mode unidirectional lasing is created for a right incident CCW mode excitation as illustrated in the lower panel of Fig. 11(b) as predicted in Figs. 4(d-f) of the Letter.

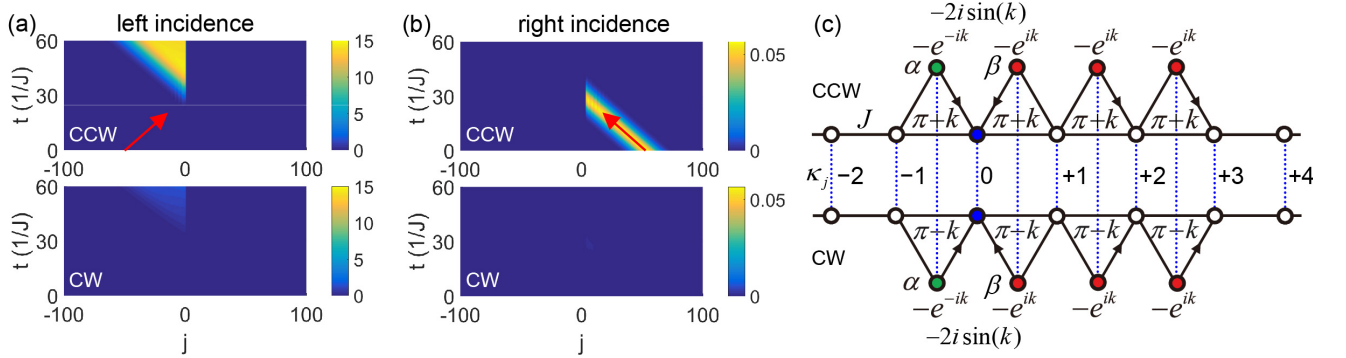


FIG. 12. Snapshots of the intensity of a transmissionless unidirectional lasing and perfect absorption for the incidences from the (a) left and (b) right. The upper (lower) panels are for the CCW (CW) mode. The initial excitation is the CCW mode Gaussian wave packet with  $\sigma = 0.1$  and wave vector  $k_c = \pi/3$ . The red arrows indicate the incidences. (c) Schematic of the system in the presence of backscattering, the coupling between the CCW and CW modes is indicated by the dotted blue lines. The system parameters are marked,  $V_0 = -2i \sin(\pi/3)$ ,  $k = \pi/3$ . The coupling phase direction is indicated by the arrows in the triangular structures, which reflect the opposite synthetic magnetic fluxes that experienced by the CCW and CW modes. In the simulations, each  $\kappa_j$  is randomly chosen within  $[0, 0.01J]$ ,  $J = 1$ ; the wave propagation dynamics are averaged over  $10^3$  sample systems.

In Figs. 12(a) and 12(b), the dynamics of a transmissionless unidirectional lasing and perfect absorption for the

CCW mode excitation is performed at weak mode coupling ( $0 \leq \kappa_j \leq 0.01J$ ). Schematic of an equivalent configuration is shown in Fig. 12(c). Notably, Fig. 12 reveals a good transmissionless unidirectional lasing and perfect absorption as depicted in Figs. 4(g-i) of the Letter. Both the CCW and CW modes lead to a simultaneous transmissionless left incident reflection divergence ( $t_L = 0$ ,  $r_L \rightarrow \infty$ ) and right incident perfect absorption ( $r_R = t_R = 0$ ). The CW mode formed in the wave propagation process of a left incident CCW mode excitation leads to a weak left-going unidirectional lasing as depicted in the lower panel of Fig. 12(a). For a right incident CCW mode excitation, both the left-going CCW mode and the CW mode formed in the wave propagation process due to the mode coupling are perfectly absorbed as depicted in the lower panel of Fig. 12(b).

---

\* jinliang@nankai.edu.cn

- [1] J. G. Muga, J. P. Palao, B. Navarro, and I. L. Egusquiza, Phys. Rep. **395**, 357 (2004).
- [2] F. Cannata, J.-P. Dedonder, and A. Ventura, Ann. Phys. **322**, 397 (2007).
- [3] Y. D. Chong, L. Ge, and A. D. Stone, Phys. Rev. Lett. **106**, 093902 (2011).
- [4] L. Feng, Y.-L. Xu, W. S. Fegadolli, M.-H. Lu, J. E. B. Oliveira, V. R. Almeida, Y.-F. Chen, and A. Scherer. Nat. Mater. **12**, 108 (2013).
- [5] H. Ramezani, H.-K. Li, Y. Wang, and X. Zhang, Phys. Rev. Lett. **113**, 263905 (2014).
- [6] H. A. Haus and W. P. Huang, Proc. IEEE **79**, 1505 (1991).
- [7] J. D. Joannopoulos, S. G. Johnson, J. N. Winn, and R. D. Meade, *Photonic Crystals: Molding the Flow of Light* (Princeton University Press, Princeton, 2008).
- [8] The directional phase factor  $e^{\pm i\phi_{\alpha,\beta}}$  in the asymmetric couplings is  $2\pi$  periodic of  $\phi_{\alpha,\beta}$ . In our discussions, when the condition  $\phi_{\alpha,\beta} = \pi \pm k$  is mentioned, we imply that  $\phi_{\alpha,\beta} + 2n\pi = \pi \pm k$  ( $n \in \mathbb{Z}$ ).
- [9] D. Jalas, A. Petrov, M. Eich, W. Freude, S. Fan, Z. Yu, R. Baets, M. Popović, A. Melloni, J. D. Joannopoulos, M. Vanwolleghem, C. R. Doerr, and H. Renner, Nat. Photon. **7**, 579 (2013).
- [10] P. Wang, L. Jin, G. Zhang, and Z. Song, Phys. Rev. A **94**, 053834 (2016).
- [11] M. Borselli, T. J. Johnson, and O. Painter, Opt. Exp. **13**, 1515 (2005).
- [12] F. Morichetti, A. Canciamilla, C. Ferrari, M. Torregiani, A. Melloni, and M. Martinelli, Phys. Rev. Lett. **104**, 033902 (2010).
- [13] J. Wiersig, Phys. Rev. A **93**, 033809 (2016).
- [14] T. J. Kippenberg, S. M. Spillane, and K. J. Vahala, Opt. Lett. **27**, 1669 (2002).
- [15] L. Jin and Z. Song, Phys. Rev. A **84**, 042116 (2011).